NTNU
Norwegian University of
Science and Technology

Magnetization dynamics of a ferromagnet embedded in a Josephson junction with a spin-orbit coupled element

Espen Kristian Wulff Wold

Master of Science in Physics and Mathematics
Submission date: June 2018
Supervisor: Jacob Rune Wüsthoff Linder, IFY

Norwegian University of Science and Technology
Department of Physics

NTNU – Trondheim
Norwegian University of
Science and Technology

Magnetization dynamics of a ferromagnet embedded in a Josephson junction with a spin-orbit coupled element

Espen Kristian Wulff Wold

June 2018

MASTER THESIS
Department of Physics
Norwegian University of Science and Technology

Supervisor: Jacob Linder

Preface

This master thesis was written during the spring semester of 2018 at the physics department of the Norwegian University of Science and Technology. It is based on a precursory work undertaken in the preceeding semester [1], but is nevertheless complete in itself.

The work was supervised by Jacob Linder of the QuSpin Center of Excellence, to whom I am grateful for his guidance, insight and remarkable diligence in always thoroughly following up on any unanswered questions left after our discussions.

Abstract

We investigate the free energy of Andreev bound states (ABS) in a Josephson junction containing a ferromagnet and an element where broken inversion symmetry produces Rashba spin-orbit coupling. Applying an extended Blonder-Tinkham-Klapwijk (BTK) formalism and finding static solutions for the wave function in the junction, we calculate the permissible energy levels in the Andreev regime and find the thermodynamic free energy. The free energy is found to depend on the magnetization direction of the ferromagnet in such a way that the effect of ABS in the junction on the magnet is an easy axis effective field, perpendicular to both the direction of broken inversion symmetry and the direction of propagation in the junction. Treating the dynamical time evolution of the system as an adiabatic perturbation, we find that the ABS effective field can be controlled by manipulating the superconductive phase across the junction and in an example system it can used to achieve switching of a magnetic bit.

Sammendrag

Vi undersøker fri energi for Andreev bundne tilstander i en Josephson-kontakt med en ferromagnet og et element der brutt inversjonssymmetri forårsaker Rashba spinnbane-kobling. Ved bruk av en utvidet Blonder-Tinkham-Klapwijk formalisme finner vi statiske løsninger for bølgefunksjonen i systemet, regner ut de mulige energinivåene i Andreev-regimet og finner den termodynamiske frie energien. Vi finner at systemets frie energi avhenger av magnetiseringsretningen i ferromagneten på en slik måte at effekten Andreev bundne tilstander i kontakten har på magnetiseringen er et effektivt felt på formen for en foretrukket magnetiseringsakse, vinkelrett på både retningen for brutt inversjonssymmetri og propagasjonsretningen i kontakten. Vi behandler den dynamiske utviklingen til systemet som en adiabatisk perturbasjon og finner at dette effektive feltet kan kontrolleres ved å styre den superledende fasen gjennom kontakten og i et eksempelsystem viser vi at dette kan utnyttes til å oppnå tilstandsendring i en magnetisk bit.

Contents

1. Introduction

Superconductivity is a an ordered low-temperature phase of many metals, in which the metal exhibits exactly zero resistance to DC currents. Simply put, what happens is that the fermionic conduction electrons form pairs that act like bosons. At low enough temperatures, these bosonic pairs will all tend to occupy the quantum state with lowest energy. In this state, the pairs collectively act as a macroscopic wave function, able to effectuate transport of pairs (and thus charge) with no resistance.

Another example of an ordered low-temperature metallic phase is ferromagnetism, though low temperatures for magnets are significantly higher than what constitutes low temperatures for superconductors. Thus we can have magnets at room temperature, while superconductivity requires cryogenic cooling. We can think of a ferromagnet as a crystal with an electron spin at each lattice point, all of which act like a tiny magnet due to the magnetic moment of the electron. Macroscopic magnets, like those used to stick notes on fridges, are the result of the alignment of a majority of the individual electron spins. The magnetization profile of a ferromagnet will in general vary spatially within the material, in a way that achieves an equilibrium between competing internal interactions. For instance, the tendency for spin alignment discourages significant change in magnetization over small distances, while the crystal structure of the material might encourage the magnetization to align with (or against) a certain crystal axis. The result can be magnetic domains (areas of uniform magnetization) oriented with or against this easy axis, separated by a transitional layer of finite width called a domain wall. If the system is disturbed from equilibrium by external interactions, we enter the realm of magnetization dynamics, describing the time evolution of possibly complex magnetization profiles.

The ferromagnetic tendency of spin alignment is at odds with pair formation in a conventional superconductor since the pairs are comprised of electrons of opposite spin, making the two phases somewhat antagonistic [2]. However, one does not need a material exhibiting both phases to observe interplay between ferromagnetism and superconductivity, as there is ample opportunity for interesting physics in structures consisting of different elements that are either superconductive or fer-

romagnetic. Such structures may be of interest in constructing spintronic devices [3], i.e. spin-electronic devices, where information is carried by spin rather than charge. Compared to conventional electronics, spintronics offer the possibility of devices that are smaller, faster and consume less power [4].

One interesting example of a system incorporating both superconductivity and ferromagnetism is the superconductor-ferromagnet-superconductor (S-F-S) junction, one configuration of which may be used to construct qubits that could be a step towards large scale quantum computing [5]. However, such (S-F-S) systems are still isotropic in spin space, in that they are indifferent to the magnetization direction of the magnetic element. As such, the magnetization dynamics of the ferromagnetic element is independent of the superconducting system.

In this thesis, we will investigate a superconducting junction with a ferromagnet and an element that breaks the isotropy in spin space, specifically a spin-orbit coupled element. The resulting spin space anisotropy is expected to couple the energy levels of the junction to the magnetization direction of the ferromagnet, and thus allow the superconductive system to influence the magnetization dynamics.

1.1 Motivation

Ferromagnetic materials have long been used for information storage, encoding bits of information in the magnetization direction of single magnetic domains. Traditionally, writing information to magnetic bits has been done by applying magnetic field generated by currents, but this approach scales poorly to the desired information densities of modern devices, since domains of decreasing size require increasingly stronger fields [6]. This makes alterative ways of manipulating magnetic domains very interesting with regards to applications. One such alternative method consists of running a spin current (a current of electrons with partially aligned spins) through the magnet, which produces a torque on the magnetization [7, 8]. In addition to requiring lower currents when the domains become small enough, this method gives better spatial accuracy as the torque arises from a current running through the actual domain rather than from an externally applied field.

Lower currents reduce resistive heating in the components, decreasing both power consumption and the need for cooling of devices. If one can somehow manipulate the magnetization of magnetic domains using a supercurrent, one could in theory avoid resistive heating entirely. The benefits of electronic devices that last longer on the same battery charge and stay cooler during operation is rather obvious from our everyday experience. Perhaps somewhat less obvious, since we rarely think of electronic devices as particularly power hungry, is the fact that more energy

efficient computation could make significant decreases to global energy consumption. For instance, it has been estimated that the power used by computations related to the cryptocurrency Bitcoin alone is on a par with the electricity consumed by the country of Ireland [9].

1.2 Scope and approach

In order to investigate the possible coupling between the magnetization of a ferromagnet and a superconductive system, we will consider a modified Josephson junction (i.e. a superconductive contact consisting of two superconductors separated by a non-superconductive element). In our modified version, the superconductors will be separated by two elements: a ferromagnet and an element that breaks spin space isotropy by Rashba spin-orbit coupling of the charge carriers. The system is depicted in Figure 1.1 as a visual reference, though it will not be explained in detail until we have covered the requisite theory.

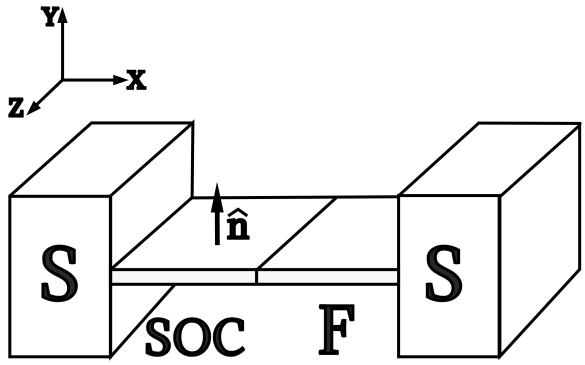

Figure 1.1: Schematic depiction of a modified Josephson junction consisting of two identical superconductors (S) separated by thin plates of 1) normal metal element with Rashba spin-orbit coupling (SOC) and 2) a ferromagnetic metal (F). The SOC element is depicted with its normal vector $\hat{\boldsymbol{n}}$, for reasons that will be elucidated in a later chapter.

Modelling the interfaces as delta function barriers of variable strength, we will investigate the system in the Andreev regime (i.e. for energies within the superconducting gap) and find the allowed energies for static solutions to the wave function for the entire junction using an extended BTK-formalism. Interpreting these allowed energies as the excitation energies of a fermionic system will allow us to calculate the free energy of the system, and crucially, how this free energy depends on the magnetization direction. The reciprocal of this dependence will give us the

effect of the superconducting system on the magnetization direction, which in turn will allow us to model the magnetization dynamic of our ferromagnetic element.

We have devoted a chapter to the theoretical foundation for each of the main physical effects in our system: superconductivity, ferromagnetism and Rashba spin-orbit coupling. Once the theory is in place, we will spend a chapter presenting and analyzing our modified Josephson junction, followed by a chapter detailing our numerical method for calculating the junction free energy. Lastly, we present and discuss our results for the free energy and magnetization dynamics and give a brief discussion of possible applications and further research.

2. Superconductivity

The phenomena of superconductivity was discovered in 1911 by H. K. Onnes when mercury displayed no resistance to DC currents if cooled below 4.2 K by the use of liquid helium [10]. Other metals were also found to exhibit this property below certain critical temperatures, and in 1933 it was found that superconductors will expel all magnetic fields as they transition to the superconducting state [11]. A microscopic theory of superconductivity proved to be elusive, but in 1956 Leon Cooper provided a key piece of the puzzle by demonstrating that electrons in a metal can form bound pairs under the influence of an attractive force [12]. The following year, Bardeen, Cooper and Schrieffer (BCS) presented a theory of superconductivity where the superconducting state is the result of electrons forming Cooper pairs [13, 14]. Our derivation of the BCS-theory will be a mean field approach inspired by [15].

2.1 BCS Hamiltonian

A system of non-interacting electrons can be described by a second quantized Hamiltonian on the form $H = \sum_{\boldsymbol{k},\sigma} \epsilon_{\boldsymbol{k}} c^\dagger_{\boldsymbol{k},\sigma} c_{\boldsymbol{k},\sigma}$, where $\epsilon_{\boldsymbol{k}} = \hbar^2 \boldsymbol{k}^2/2m - \mu$ is the energy of electron states with momentum $\boldsymbol{k}$ relative to the chemical potential μ. The operators $c^\dagger_{\boldsymbol{k},\sigma}$ and $c_{\boldsymbol{k},\sigma}$ are creation and annihilation operators of electron states with momentum $\boldsymbol{k}$ and spin σ. They obey standard commutation relations for fermions (found in e.g. [16]):

$$\{c_{\boldsymbol{k},\sigma}, c^\dagger_{\boldsymbol{k}',\sigma'}\} = \delta_{\boldsymbol{k}\boldsymbol{k}'}\delta_{\sigma\sigma'} \quad \text{and} \quad \{c_{\boldsymbol{k},\sigma}, c_{\boldsymbol{k}',\sigma'}\} = \{c^\dagger_{\boldsymbol{k},\sigma}, c^\dagger_{\boldsymbol{k}',\sigma'}\} = 0 \tag{2.1}$$

where we let curly brackets denote the anticommutator. If we now consider an attractive electron-electron interaction between the constituents of the conventional Cooper pair (i.e. electrons with opposite momenta and spin [12]) the Hamiltonian becomes:

$$H = \sum_{\boldsymbol{k},\sigma} \epsilon_{\boldsymbol{k}} c^\dagger_{\boldsymbol{k},\sigma} c_{\boldsymbol{k},\sigma} + \sum_{\boldsymbol{k},\boldsymbol{k}'} V_{\boldsymbol{k},\boldsymbol{k}'} c^\dagger_{\boldsymbol{k},\uparrow} c^\dagger_{-\boldsymbol{k},\downarrow} c_{-\boldsymbol{k}',\downarrow} c_{\boldsymbol{k}',\uparrow} \tag{2.2}$$

Taking the fluctuations around the expectation values to be small, we expand the operators in a mean field term and a fluctuation term.

$$c_{-\boldsymbol{k}',\downarrow}c_{\boldsymbol{k}',\uparrow} = \langle c_{-\boldsymbol{k}',\downarrow}c_{\boldsymbol{k}',\uparrow}\rangle + \left[c_{-\boldsymbol{k}',\downarrow}c_{\boldsymbol{k}',\uparrow} - \langle c_{-\boldsymbol{k}',\downarrow}c_{\boldsymbol{k}',\uparrow}\rangle\right] \equiv b_{\boldsymbol{k}'} + \delta b_{\boldsymbol{k}'} \tag{2.3}$$

$$c^\dagger_{\boldsymbol{k},\uparrow}c^\dagger_{-\boldsymbol{k},\downarrow} = \langle c^\dagger_{\boldsymbol{k},\uparrow}c^\dagger_{-\boldsymbol{k},\downarrow}\rangle + \left[c^\dagger_{\boldsymbol{k},\uparrow}c^\dagger_{-\boldsymbol{k},\downarrow} - \langle c^\dagger_{\boldsymbol{k},\uparrow}c^\dagger_{-\boldsymbol{k},\downarrow}\rangle\right] \equiv b^\dagger_{\boldsymbol{k}} + \delta b^\dagger_{\boldsymbol{k}} \tag{2.4}$$

where angled brackets denote expectation values. To simplify the Hamiltonian, we discard terms of second order in the fluctuations and introduce the gap parameters, given by:

$$\Delta_{\boldsymbol{k}} = \sum_{\boldsymbol{k}'} V_{\boldsymbol{k},\boldsymbol{k}'}b_{\boldsymbol{k}'} \tag{2.5}$$

$$\Delta^\dagger_{\boldsymbol{k}'} = \sum_{\boldsymbol{k}} V_{\boldsymbol{k},\boldsymbol{k}'}b^\dagger_{\boldsymbol{k}} \tag{2.6}$$

We are thus left with a Hamiltonian on the form

$$\begin{aligned}
H &= \sum_{\boldsymbol{k},\sigma}\epsilon_{\boldsymbol{k}}c^\dagger_{\boldsymbol{k},\sigma}c_{\boldsymbol{k},\sigma} + \sum_{\boldsymbol{k},\boldsymbol{k}'}V_{\boldsymbol{k},\boldsymbol{k}'}\left[b^\dagger_{\boldsymbol{k}}b_{\boldsymbol{k}'} + b^\dagger_{\boldsymbol{k}}(c_{-\boldsymbol{k}',\downarrow}c_{\boldsymbol{k}',\uparrow} - b_{\boldsymbol{k}'}) + (c^\dagger_{\boldsymbol{k},\uparrow}c^\dagger_{-\boldsymbol{k},\downarrow} - b^\dagger_{\boldsymbol{k}})b_{\boldsymbol{k}'}\right] \\
&= \sum_{\boldsymbol{k}}\epsilon_{\boldsymbol{k}}\left[1 + c^\dagger_{\boldsymbol{k},\uparrow}c_{\boldsymbol{k},\uparrow} - c_{\boldsymbol{k},\downarrow}c^\dagger_{\boldsymbol{k},\downarrow}\right] + \sum_{\boldsymbol{k}}\left[\Delta^\dagger_{\boldsymbol{k}}c_{-\boldsymbol{k},\downarrow}c_{\boldsymbol{k},\uparrow} + \Delta_{\boldsymbol{k}}c^\dagger_{\boldsymbol{k},\uparrow}c^\dagger_{-\boldsymbol{k},\downarrow} - b^\dagger_{\boldsymbol{k}}\Delta_{\boldsymbol{k}}\right] \\
&= \sum_{\boldsymbol{k}}\left[\epsilon_{\boldsymbol{k}} - b^\dagger_{\boldsymbol{k}}\Delta_{\boldsymbol{k}}\right] + \sum_{\boldsymbol{k}}\left[\epsilon_{\boldsymbol{k}}c^\dagger_{\boldsymbol{k},\uparrow}c_{\boldsymbol{k},\uparrow} - \epsilon_{\boldsymbol{k}}c_{-\boldsymbol{k},\downarrow}c^\dagger_{-\boldsymbol{k},\downarrow} + \Delta^\dagger_{\boldsymbol{k}}c_{-\boldsymbol{k},\downarrow}c_{\boldsymbol{k},\uparrow} + \Delta_{\boldsymbol{k}}c^\dagger_{\boldsymbol{k},\uparrow}c^\dagger_{-\boldsymbol{k},\downarrow}\right] \\
&= E_0 + \sum_{\boldsymbol{k}}\begin{pmatrix}c^\dagger_{\boldsymbol{k},\uparrow} & c_{-\boldsymbol{k},\downarrow}\end{pmatrix}\begin{bmatrix}\epsilon_{\boldsymbol{k}} & \Delta_{\boldsymbol{k}} \\ \Delta^\dagger_{\boldsymbol{k}} & -\epsilon_{\boldsymbol{k}}\end{bmatrix}\begin{pmatrix}c_{\boldsymbol{k},\uparrow} \\ c^\dagger_{-\boldsymbol{k},\downarrow}\end{pmatrix}
\end{aligned}$$

where we have used the commutation relations and changed the sign of the summation index in the $c_{-\boldsymbol{k},\downarrow}c^\dagger_{-\boldsymbol{k},\downarrow}$ term (which we can do as $\epsilon_{\boldsymbol{k}} = \epsilon_{-\boldsymbol{k}}$ and we sum over all $\boldsymbol{k}$). We have introduced the constant energy term $E_0 = \sum_{\boldsymbol{k}}\left[\epsilon_{\boldsymbol{k}} - b^\dagger_{\boldsymbol{k}}\Delta_{\boldsymbol{k}}\right]$, which we will ignore when concerned with the dynamics of the system. As it stands, the Hamiltonian describes a system of coupled pairs of quasiparticles: electrons with spin up, and holes resulting from the removal of a spin down electron. In anticipation of effects that lift the spin degeneracy, we would like to be able to also describe the spin-switched pairs. To that end, we change the order of the operators in each creation/annihilation term; this will only incur a sign change and the addition of a constant factor that could be absorbed into E_0. Again changing the sign of the summation index, this time in all terms, gives us

$$H = E_0' + \sum_{\boldsymbol{k}} \left[\epsilon_{\boldsymbol{k}} c^\dagger_{\boldsymbol{k},\downarrow} c_{\boldsymbol{k},\downarrow} - \epsilon_{\boldsymbol{k}} c_{-\boldsymbol{k},\uparrow} c^\dagger_{-\boldsymbol{k},\uparrow} - \Delta^\dagger_{-\boldsymbol{k}} c_{-\boldsymbol{k},\uparrow} c_{\boldsymbol{k},\downarrow} - \Delta_{-\boldsymbol{k}} c^\dagger_{\boldsymbol{k},\downarrow} c^\dagger_{-\boldsymbol{k},\uparrow} \right]$$
$$= E_0' + \sum_{\boldsymbol{k}} \begin{pmatrix} c^\dagger_{\boldsymbol{k},\downarrow} & c_{-\boldsymbol{k},\uparrow} \end{pmatrix} \begin{bmatrix} \epsilon_{\boldsymbol{k}} & -\Delta_{-\boldsymbol{k}} \\ -\Delta^\dagger_{-\boldsymbol{k}} & -\epsilon_{\boldsymbol{k}} \end{bmatrix} \begin{pmatrix} c_{\boldsymbol{k},\downarrow} \\ c^\dagger_{-\boldsymbol{k},\uparrow} \end{pmatrix}$$

Assuming that the interaction potential is on a form that makes the gap parameters momentum-independent, we can now construct a fairly simple Hamiltonian for a system described by a basis of electrons and holes with spins both up and down. Neglecting the constant energy terms, we have

$$H = \sum_{\boldsymbol{k}} \psi^\dagger_{\boldsymbol{k}} H_{\boldsymbol{k}} \psi_{\boldsymbol{k}} \tag{2.7}$$

where

$$H_{\boldsymbol{k}} = \begin{bmatrix} \epsilon_{\boldsymbol{k}} & 0 & 0 & \Delta \\ 0 & \epsilon_{\boldsymbol{k}} & -\Delta & 0 \\ 0 & -\Delta^\dagger & -\epsilon_{\boldsymbol{k}} & 0 \\ \Delta^\dagger & 0 & 0 & -\epsilon_{\boldsymbol{k}} \end{bmatrix} \quad \text{and} \quad \psi_{\boldsymbol{k}} = \begin{pmatrix} c_{\boldsymbol{k},\uparrow} \\ c_{\boldsymbol{k},\downarrow} \\ c^\dagger_{-\boldsymbol{k},\uparrow} \\ c^\dagger_{-\boldsymbol{k},\downarrow} \end{pmatrix} \tag{2.8}$$

2.2 Eigenstates of the superconducting system

The Hamiltonian for each of the decoupled subsystems can be diagonalized to find the elementary excitations of the system, and the requisite operation is a rotation of the basis called a Bogoliubov transformation [17]. To find the form of this transformation, we simply require some linear combination of the coupled operators to be an eigenstate of the Hamiltonian:

$$\begin{bmatrix} \epsilon_{\boldsymbol{k}} & \Delta e^{\mathrm{i}\phi} \\ \Delta e^{-\mathrm{i}\phi} & -\epsilon_{\boldsymbol{k}} \end{bmatrix} \begin{pmatrix} u_{\boldsymbol{k}} \\ v_{\boldsymbol{k}} e^{-\mathrm{i}\phi} \end{pmatrix} = E_{\boldsymbol{k}} \begin{pmatrix} u_{\boldsymbol{k}} \\ v_{\boldsymbol{k}} e^{-\mathrm{i}\phi} \end{pmatrix} \tag{2.9}$$

where $u^2_{\boldsymbol{k}} + v^2_{\boldsymbol{k}} = 1$ due to normalization and we have taken the superconducting phase $e^{\mathrm{i}\phi}$ out of the (complex) gap parameter so that Δ is now real. We have also taken out a phase of the second element of the eigenvector to simplify the expressions, giving:

$$\frac{u_{\boldsymbol{k}}}{v_{\boldsymbol{k}}} = \frac{\Delta}{E_{\boldsymbol{k}} - \epsilon_{\boldsymbol{k}}} \qquad \frac{v_{\boldsymbol{k}}}{u_{\boldsymbol{k}}} = \frac{\Delta}{E_{\boldsymbol{k}} + \epsilon_{\boldsymbol{k}}} \tag{2.10}$$

so that

$$E_{\boldsymbol{k}}^2 = \Delta^2 + \epsilon_{\boldsymbol{k}}^2 \tag{2.11}$$

We see that the role of the gap parameter is to prohibit arbitrarily low energies by defining a minimum energy for the system, since $E_{\boldsymbol{k}} \to \pm\Delta$ as $\epsilon_{\boldsymbol{k}} \to 0$. Additionally, we note that the allowed energies are fourfold degenerate in the momentum, with momenta $\pm k^{\pm}$ given by

$$k^{\pm} = \frac{\sqrt{2m}}{\hbar}\left[\mu \pm \sqrt{E_{\boldsymbol{k}}^2 - \Delta^2}\right]^{1/2} = k_F\left[1 \pm \frac{\sqrt{E_{\boldsymbol{k}}^2 - \Delta^2}}{\mu}\right]^{1/2} \tag{2.12}$$

and visualized in Figure 2.1 depicting the energy-momentum relations for quasiparticles in the superconductor.

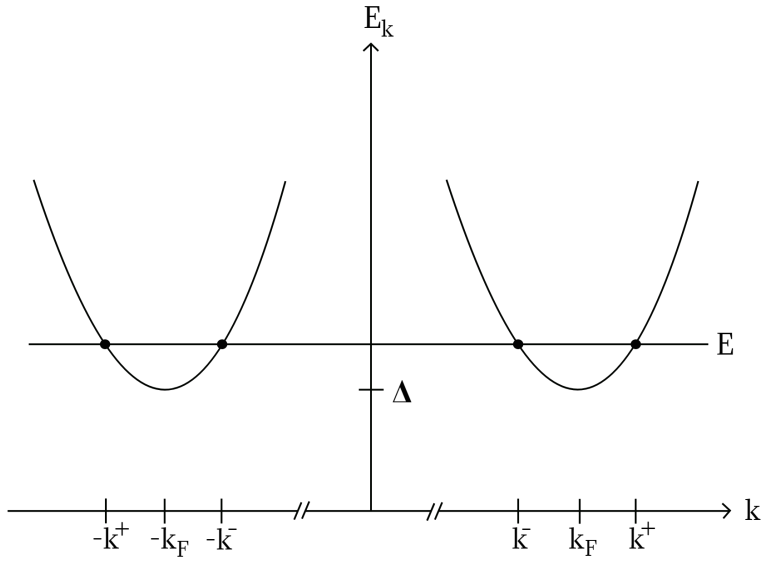

Figure 2.1: Quasiparticle excitation energies in a superconductor as a function of momentum. Δ is the energy gap of the superconductor, k_F is the Fermi momentum and $\pm k^{\pm}$ are possible quasiparticle momenta for a quasiparticle of energy E. Redrawn from source [18] and used previously in the precursor to this thesis [1].

We note that forbidden energies $E_{\boldsymbol{k}}^2 < \Delta^2$ make the momenta complex, and thus (disregarding unphysical solutions that blow up) give the wave function an exponential decay, as should be expected. Solving for the so-called coherence factors $u_{\boldsymbol{k}}$ and $v_{\boldsymbol{k}}$, gives

$$u_{\boldsymbol{k}}^2 = \frac{1}{2}\left[1+\frac{\epsilon_{\boldsymbol{k}}}{E_{\boldsymbol{k}}}\right] = \frac{1}{2}\left[1+\frac{\sqrt{E_{\boldsymbol{k}}^2-\Delta^2}}{E_{\boldsymbol{k}}}\right] \qquad v_{\boldsymbol{k}}^2 = \frac{1}{2}\left[1-\frac{\epsilon_{\boldsymbol{k}}}{E_{\boldsymbol{k}}}\right] = \frac{1}{2}\left[1-\frac{\sqrt{E_{\boldsymbol{k}}^2-\Delta^2}}{E_{\boldsymbol{k}}}\right] \quad (2.13)$$

where we have taken $\epsilon_{\boldsymbol{k}}$ to be positive. This holds for k^+ and will effectively switch the role of the two coherence factors for k^-. We thus have two eigenstates, and taking the electrons and holes to be described by plane waves, they are:

$$\psi^+ = \begin{pmatrix} u_{\boldsymbol{k}} \\ v_{\boldsymbol{k}} e^{-\mathrm{i}\phi} \end{pmatrix} e^{\mathrm{i}(\boldsymbol{k}^+\boldsymbol{r}-\omega t)} \qquad \psi^- = \begin{pmatrix} v_{\boldsymbol{k}} \\ u_{\boldsymbol{k}} e^{-\mathrm{i}\phi} \end{pmatrix} e^{\mathrm{i}(\boldsymbol{k}^-\boldsymbol{r}-\omega t)} \quad (2.14)$$

where $\omega = E_{\boldsymbol{k}}/\hbar$. The second subsystem differs only in that it requires a relative sign change in the coefficients, and for the entire system we get the four eigenstates

$$\psi_{\uparrow}^+ = \begin{pmatrix} u_{\boldsymbol{k}} \\ 0 \\ 0 \\ v_{\boldsymbol{k}} e^{-\mathrm{i}\phi} \end{pmatrix} e^{\mathrm{i}(\boldsymbol{k}^+\boldsymbol{r}-\omega t)} \quad \psi_{\uparrow}^- = \begin{pmatrix} v_{\boldsymbol{k}} \\ 0 \\ 0 \\ u_{\boldsymbol{k}} e^{-\mathrm{i}\phi} \end{pmatrix} e^{\mathrm{i}(\boldsymbol{k}^-\boldsymbol{r}-\omega t)}$$

$$\psi_{\downarrow}^+ = \begin{pmatrix} 0 \\ u_{\boldsymbol{k}} \\ -v_{\boldsymbol{k}} e^{-\mathrm{i}\phi} \\ 0 \end{pmatrix} e^{\mathrm{i}(\boldsymbol{k}^+\boldsymbol{r}-\omega t)} \quad \psi_{\downarrow}^- = \begin{pmatrix} 0 \\ v_{\boldsymbol{k}} \\ -u_{\boldsymbol{k}} e^{-\mathrm{i}\phi} \\ 0 \end{pmatrix} e^{\mathrm{i}(\boldsymbol{k}^-\boldsymbol{r}-\omega t)}$$

If we remove the superconductive characteristic of the system by letting the gap go to zero, we observe that $u_{\boldsymbol{k}} \to 1$ and $v_{\boldsymbol{k}} \to 0$, allowing us to classify the four eigenstates as electron-like (k^+) and hole-like (k^-) since they reduce to electron and hole states in the normal metal case. We have labeled the states with arrows indicating the spin of the electron or hole they reduce to as the gap parameter goes to zero.

2.3 Tunneling and the Josephson effects

As we would like to examine systems comprised of both superconductors and non-superconducting elements, we must consider transportation phenomena across interfaces between superconductors and various materials. In general, we will model such boundaries as a delta function potential, often of a strength that would classically prohibit particle transport across the interface. However, as is known from any introduction to quantum mechanics, particles can cross such barriers by quantum mechanical tunneling.

In a normal metal-insulator-normal metal (N-I-N) contact, we would expect no

net tunneling current at equilibrium, as the phase space on either side of the interface would be essentially equal. The phase space region where tunneling could occur would be the energy interval centered on the Fermi energy accessible to thermal fluctuations, as this is the range where thermally excited charge carriers could find an energetically allowed state after crossing the barrier. If we were to apply a gradually increasing voltage across the interface, tunneling in one direction would be increasingly favored energetically and we would expect to see a current linear in the voltage. However, in 1960, Ivar Giaever found that if one of the metals is a superconductor, there will be virtually no current until the voltage reaches a certain strength, above which we will again see the linear current-to-voltage relation [19, 20]. We can explain this behavior by noting that the presence of an energy gap in the superconductor means that the phase space will have a region of forbidden states centered on the Fermi energy as depicted in Figure 2.2. Therefore the voltage applied must be enough to shift the Fermi energy of the normal metal above or below this gap before there is a sufficient phase space reachable by thermal excitations that can facilitate tunneling. Indeed, this current-to-voltage relation is seen as experimental confirmation of the superconducting gap.

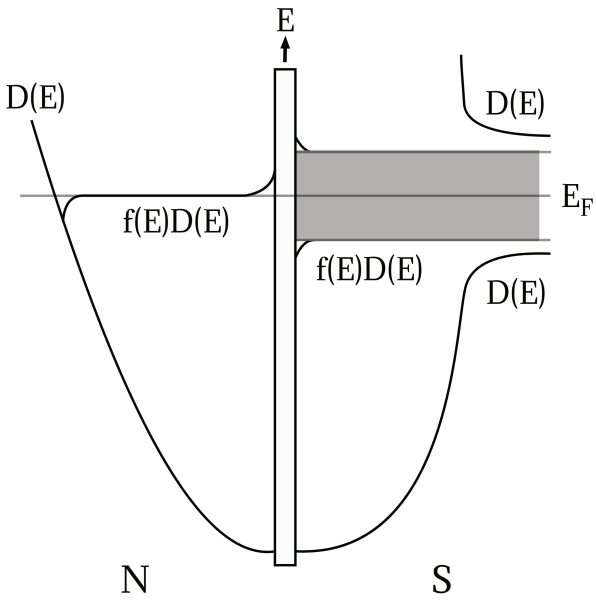

Figure 2.2: Density of states for a normal metal-insulator-superconductor (N-I-S) contact at $T \neq 0$. E_F denotes the Fermi energy, D(E) is the density of states and f(E)D(E) is the occupation of states. The gray block represents the energy gap for single particle states in the superconductor, $E_F - \Delta < E < E_F + \Delta$. Note that the thermal excitations in the normal metal fall entirely within the energy gap in the superconductor. There are a small number of thermally excited states above the energy gap in the superconductor. Redrawn from source [15] and used previously in the precursor to this thesis [1].

The tunneling across a barrier between two superconductors was in 1962 considered by B. D. Josephson [21]. He found that two superconductors separated by an insulating layer (an S-I-S contact) should exhibit a sustained DC current at zero applied voltage and that an applied constant voltage should generate an AC current. We can reproduce these results using an elegant treatment by Feynman [22], taking the superconducting state to be a collective state of the bosonic Cooper pairs described by a single wave function. It proceeds as follows: take the wavefunctions (ψ_L, ψ_R) of two identical superconductors separated by a barrier to be coupled as

$$i\hbar\frac{\partial\psi_L}{\partial t} = eV_a\psi_L + K\psi_R, \qquad i\hbar\frac{\partial\psi_R}{\partial t} = -eV_a\psi_R + K\psi_L \tag{2.15}$$

where K is a parameter describing the tendency of a pair to tunnel across the junction. A current V_a is applied across the junction, raising the energy of a pair (charge $2e$) by $2eV_a$ in the left superconductor relative to a pair in the right. Taking the wavefunctions as given by $\psi_{L(R)} = \sqrt{\rho_{L(R)}}e^{i\phi_{L(R)}}$ where ρ and ϕ are, respectively, the density of Cooper pairs and the superconductive phase, we get four equations by considering the real and imaginary parts of both equations. The imaginary parts give

$$\frac{\partial\rho_L}{\partial t} = -\frac{\partial\rho_R}{\partial t} = \frac{2K}{\hbar}\sqrt{\rho_L\rho_R}\sin(\phi_L - \phi_R) = J_1\sin\Delta\phi \tag{2.16}$$

which we identify as the current across the junction. We have introduced $\Delta\phi = \phi_L - \phi_R$ and absorbed the constants in J_1, the maximum supercurrent across the junction (we consider the system to be part of a circuit allowing current to flow through the junction with no pile up of charge so that the pair densities can be treated as constants $\rho_L = \rho_R = \rho_0$). This is the DC Josephson effect: we do not need a voltage to create a current, if there is some phase difference between the superconductors. The real part of the equations (2.15) gives us

$$\frac{\partial\Delta\phi}{\partial t} = \frac{\partial\phi_L}{\partial t} - \frac{\partial\phi_R}{\partial t} = \frac{2eV_a}{\hbar} \quad \text{or equivalently} \quad \Delta\phi = \Delta\phi_0 + \omega_J t \tag{2.17}$$

where $\Delta\phi_0$ is a constant and we have introduced the Josephson frequency $\omega_J = \frac{2eV_a}{\hbar}$. This is the AC Josephson effect: a constant voltage causes the phase difference to increase linearly with time, in turn causing a sinusoidal oscillation of the supercurrent.

For other types of Josephson junctions, the current can in general deviate from the simple sine relation on phase difference. However, since the phases are periodic, any relation on phase difference can be developed in a Fourier series:

$$J(\Delta\phi) = \sum_{n=1}^{\infty} \Big(A_n \sin(n\Delta\phi) + B_n \cos(n\Delta\phi) \Big) \tag{2.18}$$

For most junctions, symmetry considerations demand that the current is reversed if the phases of the superconductors are swapped, so that we must have

$$J(\Delta\phi) = -J(-\Delta\phi) \tag{2.19}$$

which means that we will have zero current with $\Delta\phi = 0$ and the coefficients B_n must disappear so that we are left with a series of sines. Thus, we recognize the current for the traditional (strong barrier) Josephson junction as the first term in the series

$$J(\Delta\phi) = J_1 \sin\Delta\phi + J_2 \sin(2\Delta\phi) + J_3 \sin(3\Delta\phi) + ... + J_n \sin(n\Delta\phi) \tag{2.20}$$

and expect that in general the current-phase relation could include higher order terms. The condition (2.19) can be broken in so-called ϕ_0-junctions, produced by a breaking of both time reversal and chiral symmetries in the system [23]. In such a junction the ground state is shifted by a constant phase $\phi_0 \neq 0, \pi$ yielding current-phase relations that are non-zero for $\Delta\phi = 0$ ($\phi_0 = \pi$ would amount to sign change in the coefficients, but would not break condition (2.19)).

2.4 BTK-theory and Andreev bound states

To deal with more complex cases than the traditional Josephson junction, we turn to the formalism proposed by Blonder, Tinkham and Klapwijk (BTK) in 1982 [18]. The trio considered a N-S junction with a barrier of arbitrary strength and imagined the case where an electron current is incident on the interface from within the normal metal. They then determined what reflection and transmission processes were energetically allowed, and constructed wave functions for each of the sides of the interface by combining the incident electron state and the possible reflected states in the normal metal and by combining the possible transmitted states in the superconductor. Finally, they demanded that at the interface, one should have continuity of the wave function and a discontinuity in the spatial derivative of the wave function determined by the strength of the delta function potential. This allowed them to determine the weight of each of the states representing transmissions and reflections and thus the rates of transport across the interface.

One of the reflection processes considered in the BTK paper is the so-called Andreev reflection, where an electron in a metal bordering a superconductor is re-

flected as a hole. This reflection (and the opposite process where a hole is reflected as an electron) can occur even for energies that are insufficient to excite quasiparticles in the superconductor [24]. However, even in absence of quasiparticles in the superconductor, there is obviously a transport of charge across the interface, as trading an electron (hole) for a hole (electron) entails a loss (gain) of two electrons to (from) the superconductor. We interpret this as a transfer of a Cooper pair in the ground state (i.e. at the chemical potential) into (or out of) the superconductor. This mechanism entails an intriguing possibility: a system of electrons and holes Andreev-reflected back and forth in an S-N-S junction with energies too low to be transmitted into the superconductors as quasiparticles can nevertheless facilitate transport of charge across the junction.

In a precursor to this thesis [1], we considered an S-N-S junction with such Andreev bound states. Using the BTK formalism, we constructed wave functions of electrons and holes propagating in both directions in the normal metal and (exponentially decaying) quasiparticle wave functions in the superconductors. This yielded a system of equations for the weights of the contributions from the various eigenstates. Rather than solving for the weights, we demanded only that the system be solvable, which resulted in an equation for the allowed energies of the system. These we interpreted as excitation energies of a fermionic system and used to calculate the thermodynamic free energy. The resulting expression for the free energy of the Andreev bound state system was then used to show that for a strong barrier, we should see a supercurrent proportional to $\sin\Delta\phi$, which is the expected result for a standard Josephson junction. In the main part of this thesis, we will apply this strategy to our modified Josephson junction to investigate the effect of elements that lift the spin degeneracy of the system.

3. Ferromagnetism

Ferromagnetic materials are commonly modeled as a crystal lattice where every lattice point holds an electronic magnetic moment. For metallic ferromagnets this corresponds to neglecting any magnetic contribution from the conduction electrons and considering the magnetization to be a property of the unpaired electrons localized at lattice points. We have thus defined two separate dynamics for electrons as was done by Zener in his model for ferromagnetic transition metals [25]: the itinerant (conduction) electrons in the s-orbital are (nearly) free within the metal and can effectuate transport, while the d-orbital electrons are tightly bound to the positive ions located at each lattice point.

As a lattice of electronic magnetic moments is very much a quantum system that would be cumbersome to model faithfully, we will turn to the mean field approximation of the micromagnetic model for a more convenient description. The micromagnetic model takes the material to be continuous, effectively summing over the electronic magnetic moments in small volume elements, allowing deviations from the mean field magnetization direction to cancel out. The magnitude of the magnetization vector everywhere in the material is taken to be the saturation magnetization of the material. As the tendency for single magnetic moments to deviate from the mean field direction will increase with higher temperature, we realize that the saturation magnetization must be a temperature dependent function. It has a maximum value at zero temperature, and goes to zero as one approaches the Curie temperature [26, 27] where ferromagnetism breaks down. For materials at a low, constant temperature we will take the saturation magnetization to be constant.

For the approximations of the micromagnetic model to be valid we must consider a spatial resolution where the material is not resolved in single lattice points, but rather in volume elements containing a multitude of electronic magnetic moments. Additionally, as the magnetization must be continuous at this spatial resolution, the micromagnetic model can only describe magnetization profiles that have no discernible variation over length scales comparable to the separation of lattice points.

3.1 Magnetization dynamics

The classical motion of a magnetic moment $\boldsymbol{\mu}$ in the presence of an external magnetic field $\boldsymbol{H}$ is a precession around the field given by

$$\frac{d\boldsymbol{L}}{dt} = \boldsymbol{\mu} \times \boldsymbol{H} \tag{3.1}$$

where $\boldsymbol{L}$ is the angular momentum of the magnetic moment. For a quantum description of the same situation, we turn to the operators representing the observables in question. The operator for an electronic magnetic moment can be given as

$$\hat{\mu} = -\gamma \hat{S} \tag{3.2}$$

where γ is the gyromagnetic ratio and $\hat{S}$ is the operator for electron spin. The expectation values of operators will have a time evolution given by Ehrenfest's theorem (found in any introduction to quantum mechanics, e.g. [22]). For operators with no explicit time dependence Ehrenfest gives

$$\frac{d\langle \hat{S} \rangle}{dt} = \frac{1}{i\hbar} \langle [\hat{S}, \hat{H}] \rangle \tag{3.3}$$

where brackets denote expectation values, square brackets denote the commutator and $\hat{H}$ is the Hamiltonian of the system. The Hamiltonian for an electronic magnetic moment interacting with a magnetic field is a simple Zeeman energy term,

$$\hat{H} = -\hat{\mu} \cdot \boldsymbol{H} = \gamma \hat{S} \cdot \boldsymbol{H} \tag{3.4}$$

which inserted into (3.3), gives

$$\frac{d\langle \hat{S} \rangle}{dt} = \sum_{i=x,y,z} \frac{\gamma \boldsymbol{H}_i}{i\hbar} \langle [\hat{S}, \hat{S}_i] \rangle \tag{3.5}$$

The standard commutation relations for spin operators (as can be found in e.g. [28]) are

$$[\hat{S}_x, \hat{S}_y] = \mathrm{i}\hbar \hat{S}_z \quad [\hat{S}_y, \hat{S}_z] = \mathrm{i}\hbar \hat{S}_x \quad [\hat{S}_z, \hat{S}_x] = \mathrm{i}\hbar \hat{S}_y \quad [\hat{S}_i, \hat{S}_i] = 0$$

and allow us to compute, for instance, the x-component of the commutator:

$$\sum_{i=x,y,z} \frac{\gamma \boldsymbol{H}_i}{i\hbar} \langle [\hat{S}, \hat{S}_i] \rangle_x = \sum_{i=x,y,z} \frac{\gamma \boldsymbol{H}_i}{i\hbar} \langle [\hat{S}_x, \hat{S}_i] \rangle = \gamma \big(\boldsymbol{H}_y \langle \hat{S}_z \rangle - \boldsymbol{H}_z \langle \hat{S}_y \rangle \big) = \gamma \big(\boldsymbol{H} \times \langle \hat{S} \rangle \big)_x \tag{3.6}$$

Repeating the procedure for the other components gives us

$$\frac{d\langle \hat{S} \rangle}{dt} = \gamma \boldsymbol{H} \times \langle \hat{S} \rangle = -\gamma \langle \hat{S} \rangle \times \boldsymbol{H} \quad \text{or equivalently} \quad \frac{d\langle \hat{\mu} \rangle}{dt} = -\gamma \langle \hat{\mu} \rangle \times \boldsymbol{H} \tag{3.7}$$

This is just the classical equation applied to the expectation values, since we have for an electron $\boldsymbol{L} = -\gamma \boldsymbol{\mu}$. Within the approximations of the micromagnetic model, the magnetization $\boldsymbol{M}$ at each point is proportional to the expectation value of electronic magnetic moments. Thus we can write

$$\frac{\partial \boldsymbol{M}}{\partial t} = -\gamma \boldsymbol{M} \times \boldsymbol{H} \tag{3.8}$$

This classical approximation now describes a lossless dynamic where $\boldsymbol{M}$ is in perpetual precession about the external field with a precession frequency $\omega_P = \gamma |\boldsymbol{H}|$ (as can be seen by solving for the components, for instance in the case $\boldsymbol{H} = H\hat{z}$). Physical systems however, are dissipative, and as such we would expect the magnetization to eventually align with the applied field. To introduce dissipation, Landau and Lifshitz introduced a dampening term: a small torque pointing from the magnetization towards the external field vector [29]. The result was the Landau-Lifshitz equation:

$$\frac{\partial \boldsymbol{M}}{\partial t} = -\gamma \Big[\boldsymbol{M} \times \boldsymbol{H} + \frac{\alpha}{M_S} \boldsymbol{M} \times (\boldsymbol{M} \times \boldsymbol{H}) \Big] \tag{3.9}$$

$M_s = |\boldsymbol{M}|$ is the saturation magnetization and α is a small dimensionless constant denoting the strength of the damping. α is determined phenomenologically, and as such includes damping caused by energy loss to any relevant microscopic mechanism. Examples include energy lost as excitations of phonons and as kinetic energy to conduction electrons. Assuming that the energy loss is isotropic and uniform in the material, the specifics are of no concern to us with regards to the magnetization dynamics. Gilbert updated the equation with a new damping term that would better describe the effects of stronger damping [30], resulting in the Landau-Lifshitz-Gilbert (LLG) equation:

$$\frac{\partial \boldsymbol{M}}{\partial t} = -\gamma \Big[\boldsymbol{M} \times \boldsymbol{H} - \frac{\alpha}{M_S} \boldsymbol{M} \times \frac{\partial \boldsymbol{M}}{\partial t} \Big] \tag{3.10}$$

Anticipating the need for numerical calculations, we make the equation dimensionless by dividing by γM_s^2 and introducing a new time scale $1/(\gamma M_s)$ and the di-

mensionless variables $\boldsymbol{m} = \boldsymbol{M}/M_s$, $\boldsymbol{h} = \boldsymbol{H}/M_s$. (For SI units we would divide by $\mu_0\gamma M_s^2$ instead.)

$$\frac{\partial \boldsymbol{m}}{\partial t} = -\boldsymbol{m}\times\boldsymbol{h} + \alpha\,\boldsymbol{m}\times\frac{\partial \boldsymbol{m}}{\partial t} \tag{3.11}$$

Additionally, we would like to gather all time derivatives on the left, so we try to make sense of the last term, writing

$$\boldsymbol{m}\times\frac{\partial \boldsymbol{m}}{\partial t} = -\boldsymbol{m}\times(\boldsymbol{m}\times\boldsymbol{h}) + \alpha\,\boldsymbol{m}\times\left(\boldsymbol{m}\times\frac{\partial \boldsymbol{m}}{\partial t}\right) = -\boldsymbol{m}\times(\boldsymbol{m}\times\boldsymbol{h}) - \alpha\frac{\partial \boldsymbol{m}}{\partial t} \tag{3.12}$$

where in the last equality we have used the identity $\boldsymbol{A}\times(\boldsymbol{B}\times\boldsymbol{C}) = (\boldsymbol{A}\cdot\boldsymbol{C})\boldsymbol{B} - (\boldsymbol{A}\cdot\boldsymbol{B})\boldsymbol{C}$ and the fact that $\boldsymbol{m}\cdot\boldsymbol{m} = 1$ and $\boldsymbol{m}\cdot\frac{\partial \boldsymbol{m}}{\partial t} = 0$ (the time derivative is always perpendicular to the magnetization). Inserting this result into (3.11) we get

$$\frac{\partial \boldsymbol{m}}{\partial t} = -\boldsymbol{m}\times\boldsymbol{h} + \alpha\left(-\boldsymbol{m}\times(\boldsymbol{m}\times\boldsymbol{h}) - \alpha\frac{\partial \boldsymbol{m}}{\partial t}\right) \tag{3.13}$$

$$(1+\alpha^2)\frac{\partial \boldsymbol{m}}{\partial t} = -\boldsymbol{m}\times\left(\boldsymbol{h} + \alpha\,\boldsymbol{m}\times\boldsymbol{h}\right) \tag{3.14}$$

3.2 Effective field formalism

To this point we have considered only the effect of an external magnetic field, which allows us to describe rather simple systems. Interestingly, any torque felt by the magnetization can be included by replacing the external field with an effective field incorporating the effect of the torque. Our treatment will follow Gilbert [30], defining the potential energy density of the magnetization under rotation in the presence of any such torques, $U(\boldsymbol{M})$. The effective field is then

$$\boldsymbol{H}_{\text{eff}} = -\frac{\partial U(\boldsymbol{M})}{\partial \boldsymbol{M}} \tag{3.15}$$

For an external field $\boldsymbol{H}_{\text{e}}$, we have a Zeeman energy density

$$U_{\text{e}}(\boldsymbol{M}) = -\boldsymbol{M}\cdot\boldsymbol{H}_{\text{e}} \qquad \text{giving} \qquad -\frac{\partial U(\boldsymbol{M})}{\partial \boldsymbol{M}} = \boldsymbol{H}_{\text{e}} \tag{3.16}$$

which is obviously what we want. As differentiation distributes over sums, we can simply calculate the effective field resulting from various interactions and add them all up to produce the total effective field. For other contributions to the effective field, the energy can depend on the magnetization profile over the whole sample, and we must redefine the effective field as a functional derivative of the energy functional $U[\boldsymbol{M}]$.

$$\boldsymbol{H}_{\text{eff}} = -\frac{\delta U[\boldsymbol{M}]}{\delta \boldsymbol{M}} \tag{3.17}$$

The energy contribution for an external field will then be

$$U_{\text{e}}[\boldsymbol{M}] = -\int \left[\boldsymbol{M} \cdot \boldsymbol{H}_{\text{e}}\right] \mathrm{d}\boldsymbol{r} \tag{3.18}$$

producing the same effective field term as the earlier formulation. There are five interactions contributing to the potential energy given by Gilbert:

$$U[\boldsymbol{M}] = U_{\text{e}}[\boldsymbol{M}] + U_{\text{ex}}[\boldsymbol{M}] + U_{\text{d}}[\boldsymbol{M}] + U_{\text{a}}[\boldsymbol{M}] + U_{\text{me}}[\boldsymbol{M}] \tag{3.19}$$

The contributions following the external field are, respectively, the exchange energy, the demagnetization energy, the anisotropy energy and the magnetoelastic energy.

3.2.1 Exchange energy

The exchange energy is the potential energy of the direct interaction between electron spins, which in ferromagnets favors parallel spin alignment. We can understand this energy as an electrostatic energy by noting that for two electrons, a symmetric (antisymmetric) spin distribution demands an antisymmetric (symmetric) spatial wave function to make the total wave function antisymmetric as demanded by the Pauli exclusion principle [31]. Thus, the charge distribution (and hence the electrostatic energy) will depend on the relative orientations of the electron spins. The exchange interaction between two electrons can be modeled by a Heisenberg Hamiltonian:

$$\hat{H}_H = -2J\hat{S}_i \cdot \hat{S}_j \tag{3.20}$$

where $\hat{S}_i, \hat{S}_j$ are the spin operators for electrons i, j and J is the exchange integral (positive for ferromagnets). As this interaction depends on overlap of electron wave functions, it is quite short ranged, and can be taken to apply only to nearest neighbors as a first approximation. Considering a classical model for this interaction (i.e. substituting classical spin vectors for the operators) gives us an energy that is clearly minimized for parallel spins:

$$E = -2JS^2\cos\theta \quad \geq \quad E_0 = -2JS^2 \tag{3.21}$$

where θ is the angle between the spin vectors and S is their magnitude. As the approximations of the micromagnetic model allow only miniscule changes in the magnetization direction over the distance separating single magnetic moments, we

can express the angle dependence as a Taylor expansion truncated at second order: $\cos\theta \approx 1-\theta^2/2$ giving

$$\delta E = E - E_0 = -2JS^2(1-\theta^2/2-1) = JS^2\theta^2 \tag{3.22}$$

With lattice spacing a between neighboring electrons, we can identify the angle between neighboring spins with the gradient of the magnetization:

$$|\nabla \boldsymbol{M}| \approx \frac{\theta M_s}{a} \tag{3.23}$$

$$\delta E = \frac{JS^2a^2}{M_s^2}(\nabla \boldsymbol{M})^2 \tag{3.24}$$

Finally, we can get the contribution to the potential energy by integrating over the material volume, giving

$$U_{\text{ex}}[\boldsymbol{M}] = \frac{A}{M_s^2}\int \left[(\nabla \boldsymbol{M})^2\right]\mathrm{d}\boldsymbol{r} \qquad \text{and} \qquad \boldsymbol{H}_{\text{ex}} = -\frac{\delta U_{\text{ex}}[\boldsymbol{M}]}{\delta \boldsymbol{M}} = \frac{2A}{M_s^2}\nabla^2\boldsymbol{M} \tag{3.25}$$

where $A>0$ is the exchange stiffness. In calculating the effective field, we have dropped a surface term proportional to $\nabla \boldsymbol{M}$, effectively demanding that the magnetization gradient vanishes on the boundary of the material. We note that $\frac{2A}{M_s^2}$ ($\frac{2A}{\mu_0 M_s^2}$ in SI units) must have dimension length squared, allowing us to define a characteristic length scale for the magnetization profile called the exchange length: $l_{\text{ex}} = \frac{\sqrt{2A}}{M_s}$. The magnetization profile can be expected to be approximately constant over distances comparable to the exchange length, which in transition metals is typically on the order of 1-10 nanometers [32].

3.2.2 Demagnetization energy

The demagnetization energy is due to the interaction between the magnetization and the demagnetizing field $\boldsymbol{H}_{\text{d}}$, generated by the magnetization of the magnetic material:

$$U_{\text{d}} = -\frac{1}{2}\int \left[\boldsymbol{M}\cdot\boldsymbol{H}_{\text{d}}\right]\mathrm{d}\boldsymbol{r} \tag{3.26}$$

However, the form of $\boldsymbol{H}_{\text{d}}$ depends both on the magnetization profile and the shape of the magnet, and often cannot be found analytically. It is given for an ellipsoid by Stoner and Wohlfart [33] as:

$$U_{\text{d}} = \frac{1}{2}\int \left[N_xM_x^2 + N_yM_y^2 + N_zM_z^2\right]\mathrm{d}\boldsymbol{r} \tag{3.27}$$

where N_i are the demagnetization coefficients along the axes of the ellipsoid. In the limit of a prolate spheroid elongated along the x-axis so that it approaches a cylindrical shape, we get $N_x << N_y = N_z \equiv N_\perp$ and

$$U_\mathrm{d} = \frac{1}{2}\int \left[N_\perp (M_y^2 + M_z^2)\right] \mathrm{d}\boldsymbol{r} = -\frac{K}{M_s^2}\int M_x^2 \mathrm{d}\boldsymbol{r} \tag{3.28}$$

where in the last equality we have used that the length of the magnetization vector is constant, subtracted a constant energy term and introduced a new constant K of dimension energy density. The effective field would then be

$$\boldsymbol{H}_\mathrm{d} = \frac{2K}{M_s^2} M_x \hat{x} \tag{3.29}$$

Such a field is called an easy x-axis, as it would drive the magnetization towards $\pm\hat{x}$ (depending on the initial sign of M_x).

3.2.3 Anisotropy energy

The crystal lattice of a ferromagnet will in in general have certain symmetries that make some magnetization directions more energetically favorable than others. This difference in energy for different relative orientations of the magnetization and the crystal axes is called the anisotropy energy (or magnetocrystalline energy, to separate it from anisotropic contributions from e.g. demagnetization energy). We can understand this coupling between real space and spin space by noting that spin-orbit coupling will cause the charge distributions of electrons in the lattice to have an asymmetry tied to the direction of the spin [27]. Since the crystal axes give the positions of neighboring electrons, the relative angle of spins in relation to the crystal axes will determine the overlap of charge distributions and thus electrostatic energy.

To first order, the anisotropy energy of cubic and hexagonal lattice structures can be given on the form [27]:

$$U_\mathrm{a,\,cubic} = \frac{K_1}{M_s^4}\int \left[M_x^2 M_y^2 + M_y^2 M_z^2 + M_z^2 M_x^2\right] \mathrm{d}\boldsymbol{r} \tag{3.30}$$

$$U_\mathrm{a,\,hex} = -\frac{K_2}{M_s^2}\int M_x^2 \mathrm{d}\boldsymbol{r} \tag{3.31}$$

where the cubic axes are along x, y, z and the hexagonal axis is in the x-direction. The constants introduced are both of dimension energy density. We note that the hexagonal anisotropy energy takes the form of an easy axis.

3.2.4 Magnetoelastic energy

The magnetoelastic energy is due to a coupling between magnetization direction and strains on the crystal lattice. A crystal lattice under mechanical strain can be deformed, resulting in a change in crystal geometry. This can in turn change the anisotropy energy discussed above, and thus the magnetization. When such a coupling exists, the converse effect must also be possible: the magnetization can put strains on the lattice and cause it to deform. This process is called magnetostriction. The magnetoelastic energy for a cubic lattice can be formulated as a contribution to the anisotropy energy:

$$U_{\text{a, cubic}} + U_{\text{me}} = \frac{K_1 + K_{\text{me}}}{M_s^4} \int \left[M_x^2 M_y^2 + M_y^2 M_z^2 + M_z^2 M_x^2 \right] \mathrm{d}\boldsymbol{r} \tag{3.32}$$

where the constant K_{me} depends on the elastic and magnetostriction properties of the material and is typically small ($K_{\text{me}}/K_1 \approx 10^{-3}$ for iron) [34].

4. Rashba spin-orbit coupling

Spin-orbit coupling is an interaction between the momentum and spin of a particle, taking its name from instances like the hydrogen atom where it manifests as a coupling between spin and orbital angular momentum. If we consider an electron moving in the radial electric field of the nucleus, relativistic effects will cause the electron to experience a magnetic field. A constant electric field in the lab frame will cause a moving frame to experience a magnetic field given by [35]

$$\boldsymbol{B} = -\frac{\gamma}{c}(\boldsymbol{v} \times \boldsymbol{E}) \approx -\frac{\boldsymbol{v} \times \boldsymbol{E}}{c} = -\frac{\boldsymbol{k} \times \boldsymbol{E}}{cm_e} \tag{4.1}$$

where c is the speed of light, $\boldsymbol{v}, \boldsymbol{k}$ and m_e are the electron velocity, momentum and mass, respectively, and $\boldsymbol{E}$ is the electric field in the lab frame. The Lorentz factor γ can be approximated as unity in the non-relativistic limit. Inserting $\boldsymbol{E} = |E|\hat{\boldsymbol{r}}$ (where $\hat{\boldsymbol{r}}$ is the radial unit vector) then gives

$$\boldsymbol{B} \approx -\frac{|E|}{cm_e}\boldsymbol{k} \times \hat{\boldsymbol{r}} = \frac{|E|}{cm_e}\boldsymbol{L} \tag{4.2}$$

where $\boldsymbol{L}$ is the orbital angular momentum. The electron will then have a Zeeman energy $-\boldsymbol{\mu_e} \cdot \boldsymbol{B} \propto \boldsymbol{S} \cdot \boldsymbol{L}$ where $\boldsymbol{S}$ is the electron spin, making the coupling between spin and orbital angular momentum explicit.

4.1 Rashba effect

We will be interested in Rashba spin orbit coupling, where the electric field is caused by a broken inversion symmetry in a crystal. Considering a crystal with broken inversion symmetry in the x-direction (i.e. the crystal looks different in directions $\pm\hat{\boldsymbol{x}}$), there can be a potential difference along the x-direction: $V(x) \neq V(x + \Delta x)$. This asymmetry in the potential produces a non-zero gradient. A rigorous microscopic derivation of the Rashba effect would have to take into account the exact form of this possibly complicated asymmetric potential. For our purposes however, it will suffice to approximate the gradient as the first order of a Taylor expansion and

model it as a constant electric field in the direction of broken symmetry.

Such a constant electric field should give a moving electron a spin dependent energy term as seen for the hydrogen atom above. Bychkov and Rashba [36] investigated the lifting of spin degeneracy in the presence of broken inversion symmetry and found it to be described by the Rashba Hamiltonian:

$$H_R = \alpha_R \boldsymbol{\sigma} \cdot (\boldsymbol{k} \times \hat{\boldsymbol{n}}) \tag{4.3}$$

where α_R is a constant denoting the strength of the interaction, $\boldsymbol{\sigma} = \sigma_x \hat{\boldsymbol{x}} + \sigma_y \hat{\boldsymbol{y}} + \sigma_z \hat{\boldsymbol{z}}$ are the Pauli spin matrices and $\hat{\boldsymbol{n}}$ is a unit vector in the direction of broken symmetry. In our simple model $\boldsymbol{E} = |E|\hat{\boldsymbol{n}}$, we can write $\boldsymbol{k} \times \hat{\boldsymbol{n}} \propto \boldsymbol{B}$ where $\boldsymbol{B}$ is the magnetic field in the electron frame as defined above. Thus we see that the Rashba Hamiltonian describes a Zeeman energy term $H_R \propto \boldsymbol{\sigma} \cdot \boldsymbol{B}$ as we expect from the discussion of the hydrogen atom. We note that the energy splitting will be proportional to the component of $\boldsymbol{k}$ perpendicular to the direction of broken symmetry, so that if $\hat{\boldsymbol{n}} = \hat{\boldsymbol{y}}$ and $\boldsymbol{k} = k\hat{\boldsymbol{x}}$ we get

$$H_R = \alpha_R k \boldsymbol{\sigma} \cdot (\hat{\boldsymbol{x}} \times \hat{\boldsymbol{y}}) = \alpha_R k \boldsymbol{\sigma} \cdot \hat{\boldsymbol{z}} = \alpha_R k \sigma_z \tag{4.4}$$

Such an energy splitting would displace the Fermi surface of spin-up and spin-down electrons in opposite directions, as illustrated for a normal metal with Rashba SOC in Figure 4.1. The magnitude of Rashba coupling varies several orders of magnitude for different materials, with a low value example $\alpha_R \approx 0.05$ eVÅ (Å $= 10^{-10}$m denotes the Ångström) found for a quasi-two-dimensional electron gas at a heterointerface [37]. Significantly larger values appear on the surfaces of heavy metals: for surface states in Au(111) and Bi(111) Rashba parameters of $\alpha_R \approx 0.3$ eVÅ and $\alpha_R \approx 0.6$ eVÅ, respectively, have been found [38, 39]. An investigation of a Bi/Au surface alloy showed an even stronger Rashba splitting with $\alpha_R \approx 3$ eVÅ [40].

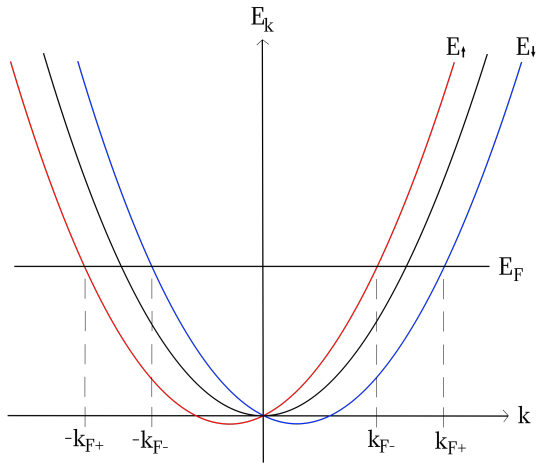

Figure 4.1: Energy-momentum relation displaying the spin splitting of the Fermi surface in a normal metal with Rashba spin-orbit coupling. The electron momentum is taken to be in the x-direction, and inversion symmetry is broken in the y-direction. Arrow subscripts denote spin, with spin-up being in the z-direction. The Fermi surface for spin-up is shifted from $[-k_F, k_F]$ to $[-k_{F+}, k_{F-}]$ while spin-down goes to $[-k_{F-}, k_{F+}]$. Used previously in the precursor to this thesis [1].

5. Modified Josephson junction: S-SOC-F-S

The system to be investigated in the remainder of this thesis will be a modified Josephson junction, incorporating a normal metal element with Rashba spin-orbit coupling (SOC) and a ferromagnetic metal element. The junction is illustrated schematically in Figure 5.1. The superconducting elements are conventional superconductors as described in Chapter 2, and the junction is taken to be short enough to allow supercurrent transport by Andreev bound states. We are only interested in transport across the junction (along $\pm\hat{\boldsymbol{x}}$) and will treat the system as one-dimensional in real space. Although the SOC and F elements are geometrically similar, we will neglect any Rashba SOC due to broken inversion symmetry in the ferromagnet. As we saw in Chapter 4, the magnitude of Rashba SOC varies over several orders of magnitude, and we assume the material chosen as the ferromagnetic element will produce negligible Rashba effects. We did initially try to solve a system where the ferromagnet was spin-orbit coupled, but the resulting expressions were hopelessly cumbersome. The approximation above was chosen mainly to avoid this time-demanding model of the system, with the hope that it will not alter the essential physics of the system.

5.1 Eigenstates of junction elements

To apply the BTK-formalism to this system, we must first find the eigenstates of the different elements. To this end, we will apply the four-spinor formalism from Chapter 2, effectively choosing a basis of electrons and holes with spin resolved in the z-direction. We will be interested in the Hamiltonian matrices H_k given by

$$H = \sum_k \psi_k^\dagger H_k \psi_k \qquad \text{where} \qquad \psi_k = \begin{pmatrix} c_{k\uparrow} \\ c_{k\downarrow} \\ c_{-k\uparrow}^\dagger \\ c_{-k\downarrow}^\dagger \end{pmatrix} \tag{5.1}$$

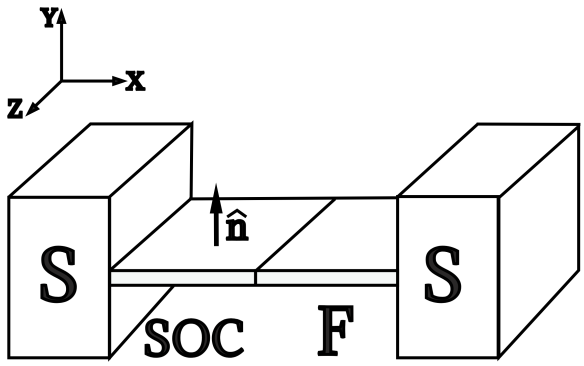

Figure 5.1: Schematic depiction of a modified Josephson junction consisting of two identical superconductors (S) separated by thin plates of 1) a normal metal element with Rashba spin-orbit coupling (SOC) and 2) a ferromagnetic metal (F). The plates are in the x-z plane, and thus has broken inversion symmetry along the plane normal $\hat{\boldsymbol{n}} = \hat{\boldsymbol{y}}$.

where the creation and annihilation operators are taken to produce plane waves in the x-direction. For the superconductors, we have seen that the Hamiltonian takes the form

$$H_{S,k} = \begin{bmatrix} \epsilon_k & 0 & 0 & \Delta e^{i\phi} \\ 0 & \epsilon_k & -\Delta e^{i\phi} & 0 \\ 0 & -\Delta e^{-i\phi} & -\epsilon_k & 0 \\ \Delta e^{-i\phi} & 0 & 0 & -\epsilon_k \end{bmatrix} \tag{5.2}$$

where $\Delta > 0$ is the gap energy. Solving the time-independent Schrödinger equation for this Hamiltonian yields eigenfunctions

$$\psi^+_\uparrow = \begin{pmatrix} u_k \\ 0 \\ 0 \\ v_k e^{-i\phi_{L(R)}} \end{pmatrix} e^{\pm ik^+ x} \qquad \psi^-_\uparrow = \begin{pmatrix} v_k \\ 0 \\ 0 \\ u_k e^{-i\phi_{L(R)}} \end{pmatrix} e^{\pm ik^- x}$$

$$\psi^+_\downarrow = \begin{pmatrix} 0 \\ u_k \\ -v_k e^{-i\phi_{L(R)}} \\ 0 \end{pmatrix} e^{\pm ik^+ x} \qquad \psi^-_\downarrow = \begin{pmatrix} 0 \\ v_k \\ -u_k e^{-i\phi_{L(R)}} \\ 0 \end{pmatrix} e^{\pm ik^- x}$$

for the left (right) superconductor with phase ϕ_L (ϕ_R). To remind ourselves that they are both very close to the Fermi momentum, we write the momenta as

$$k^{\pm} = k_F\left[1 \pm \frac{\Delta}{\mu}\sqrt{\frac{E^2}{\Delta^2} - 1}\right]^{1/2} = k_F\left[1 \pm \widetilde{\Delta}\sqrt{\frac{E^2}{\Delta^2} - 1}\right]^{1/2} \tag{5.3}$$

where $\widetilde{\Delta}$ is a (small) dimensionless energy parameter. Considering that the group velocity $v_g = \frac{\partial E}{\partial \hbar k}$ is positive for $+k^+, -k^-$ and negative for $-k^+, +k^-$ (as seen in Figure 2.1), we note that the hole-like excitations propagate in the direction opposite their momenta.

For the SOC-element, we have the diagonal Hamiltonian

$$\begin{aligned} H &= \sum_{\text{electrons}} (H_e + H_R) = \sum_{k,\sigma} (\epsilon_k + \alpha_R k \sigma_z) c^{\dagger}_{k,\sigma} c_{k,\sigma} \\ &= \sum_k \left[(\epsilon_k + \alpha_R k) c^{\dagger}_{k,\uparrow} c_{k,\uparrow} + (\epsilon_k - \alpha_R k) c^{\dagger}_{k,\downarrow} c_{k,\downarrow} \right] \end{aligned}$$

where H_e is the non-interacting electron energy given simply by ϵ_k and H_R is the Rashba Hamiltonian given in (4.4). We have used that σ_z has eigenvalue $+(-)1$ for spin-up(down). Fermion commutation relations entail a sign change (and a constant energy term we ignore) going from $c^{\dagger}_{k,\sigma} c_{k,\sigma}$ to $c_{k,\sigma} c^{\dagger}_{k,\sigma}$, while changing the sign of k (going from $c_{k,\sigma} c^{\dagger}_{k,\sigma}$ to $c_{-k,\sigma} c^{\dagger}_{-k,\sigma}$) entails a sign change only for the Rashba term. Hence, we get the Hamiltonian matrix

$$H_{SOC,k} = \begin{bmatrix} \epsilon_k + \alpha_R k & 0 & 0 & 0 \\ 0 & \epsilon_k - \alpha_R k & 0 & 0 \\ 0 & 0 & -\epsilon_k + \alpha_R k & 0 \\ 0 & 0 & 0 & -\epsilon_k - \alpha_R k \end{bmatrix} \tag{5.4}$$

whose eigenfunctions are obviously trivial spinors. However, we note that the excitation energies are not indifferent to the sign of k, giving for positive momentum

$$\begin{aligned} k_{c_{k\uparrow}} &= \frac{\sqrt{\alpha_R^2 m^2 + 2m\hbar^2(\mu + E)} - \alpha_R m}{\hbar^2} = k_F\left[\sqrt{\frac{\alpha_R^2 m}{2\mu\hbar^2} + 1 + \frac{E}{\mu}} - \frac{\alpha_R}{\hbar}\sqrt{\frac{m}{2\mu}}\right] \\ &= k_F\left[\sqrt{\widetilde{\alpha}^2 + 1 + \frac{E}{\mu}} - \widetilde{\alpha}\right] \equiv k_1 \end{aligned}$$

where we have introduced the dimensionless energy parameter $\widetilde{\alpha}$ denoting the strength of Rashba coupling. The subscript refers to the non-zero element in the trivial spinor to which the momentum belongs. For the other spinors the sign of E and $\widetilde{\alpha}$ in the momentum expression is given by, respectively, the sign of ϵ_k and the

relative sign of ϵ_k and $\alpha_R k$ in the appropriate Hamiltonian element.

$$k_{c_{k\downarrow}} = k_F\left[\sqrt{\tilde{\alpha}^2+1+\frac{E}{\mu}}+\tilde{\alpha}\right] \equiv k_2$$

$$k_{c^\dagger_{-k\uparrow}} = k_F\left[\sqrt{\tilde{\alpha}^2+1-\frac{E}{\mu}}+\tilde{\alpha}\right] \equiv k_3$$

$$k_{c^\dagger_{-k\downarrow}} = k_F\left[\sqrt{\tilde{\alpha}^2+1-\frac{E}{\mu}}-\tilde{\alpha}\right] \equiv k_4$$

For negative momenta, the relative sign of the two terms in the elements of the Hamiltonian changes, which in turn switches the roles of k_1 and k_2 and the roles of k_3 and k_4, giving

$$k_{c_{k\uparrow}} = k_2 \qquad k_{c_{k\downarrow}} = k_1 \qquad k_{c^\dagger_{-k\uparrow}} = k_4 \qquad k_{c^\dagger_{-k\downarrow}} = k_3$$

The eight different eigenstates in the SOC-element are then

$$\psi_1 = \begin{pmatrix}1\\0\\0\\0\end{pmatrix} e^{\mathrm{i}k_1 x} \qquad \psi_2 = \begin{pmatrix}0\\1\\0\\0\end{pmatrix} e^{\mathrm{i}k_2 x} \qquad \psi_3 = \begin{pmatrix}0\\0\\1\\0\end{pmatrix} e^{\mathrm{i}k_3 x} \qquad \psi_4 = \begin{pmatrix}0\\0\\0\\1\end{pmatrix} e^{\mathrm{i}k_4 x}$$

$$\psi_5 = \begin{pmatrix}1\\0\\0\\0\end{pmatrix} e^{-\mathrm{i}k_2 x} \qquad \psi_6 = \begin{pmatrix}0\\1\\0\\0\end{pmatrix} e^{-\mathrm{i}k_1 x} \qquad \psi_7 = \begin{pmatrix}0\\0\\1\\0\end{pmatrix} e^{-\mathrm{i}k_4 x} \qquad \psi_8 = \begin{pmatrix}0\\0\\0\\1\end{pmatrix} e^{-\mathrm{i}k_3 x}$$

Finally, for the ferromagnetic element with magnetization $\boldsymbol{M} = M_s\boldsymbol{m}$ our particles will have the standard non-interacting electron energy ϵ_k, and some energy term due to the interaction of the electronic magnetic moment and the magnetization. The significant part of this interaction will be a quantum mechanical exchange interaction corresponding to that between the spins in the lattice (the classical interaction with the magnetization field is negligible in comparison). We can nevertheless model this interaction as a magnetic moment interacting with an effective field $\boldsymbol{H}_{\text{eff}} \propto \boldsymbol{M}$ giving the Hamiltonian a term

$$H_{\text{mag}} = -\boldsymbol{H}_{\text{eff}} \cdot \boldsymbol{\mu}_e = h\boldsymbol{m}\cdot\boldsymbol{\sigma} = h(m_x\sigma_x + m_y\sigma_y + m_z\sigma_z) \tag{5.5}$$

where we have used that the electronic magnetic moment is antiparallel to the electron spin. We have absorbed all dimensionful constants into h, a parameter

of dimension energy denoting the strength of the exchange interaction. Note that we have approximated the ferromagnet as a single magnetic domain, which will be accurate as long as the dimensions of the magnet are comparable to the magnetic exchange length. If our basis were spin-resolved in the direction of magnetization we would simply get an energy $\pm h$ added to the ϵ_k energies and the Hamiltonian would be diagonal. However, we would like to describe the system for an arbitrary magnetization direction and so have to consider the effects of $\boldsymbol{m}\cdot\boldsymbol{\sigma}$ on the spin-up and spin-down states resolved in the z-direction. Using the standard form of the Pauli matrices, we have

$$\sigma_x|\uparrow\rangle = \begin{bmatrix}0 & 1\\ 1 & 0\end{bmatrix}\begin{pmatrix}1\\0\end{pmatrix} = \begin{pmatrix}0\\1\end{pmatrix} = |\downarrow\rangle \qquad \sigma_y|\uparrow\rangle = \begin{bmatrix}0 & -\mathrm{i}\\ \mathrm{i} & 0\end{bmatrix}\begin{pmatrix}1\\0\end{pmatrix} = \begin{pmatrix}0\\\mathrm{i}\end{pmatrix} = \mathrm{i}|\downarrow\rangle \qquad \sigma_z|\uparrow\rangle = |\uparrow\rangle \tag{5.6}$$

$$\sigma_x|\downarrow\rangle = \begin{bmatrix}0 & 1\\ 1 & 0\end{bmatrix}\begin{pmatrix}0\\1\end{pmatrix} = \begin{pmatrix}1\\0\end{pmatrix} = |\uparrow\rangle \qquad \sigma_y|\downarrow\rangle = \begin{bmatrix}0 & -\mathrm{i}\\ \mathrm{i} & 0\end{bmatrix}\begin{pmatrix}0\\1\end{pmatrix} = \begin{pmatrix}-\mathrm{i}\\0\end{pmatrix} = -\mathrm{i}|\uparrow\rangle \qquad \sigma_z|\downarrow\rangle = -|\downarrow\rangle \tag{5.7}$$

showing that the misalignment of magnetization and spin axis generates spin transitions:

$$\boldsymbol{m}\cdot\boldsymbol{\sigma}|\uparrow\rangle = m_z|\uparrow\rangle + (m_x + \mathrm{i}m_y)|\downarrow\rangle \tag{5.8}$$

$$\boldsymbol{m}\cdot\boldsymbol{\sigma}|\downarrow\rangle = -m_z|\downarrow\rangle + (m_x - \mathrm{i}m_y)|\uparrow\rangle \tag{5.9}$$

The Hamiltonian we get is then, for the electrons:

$$\begin{aligned}
H_F^e &= \sum_{k,\sigma,k',\sigma'} \langle k,\sigma|\epsilon_k + h\boldsymbol{m}\cdot\boldsymbol{\sigma}\,|k',\sigma'\rangle\, c^\dagger_{k,\sigma}c_{k',\sigma'}\\
&= \sum_{k,\sigma}\Big[\langle k,\sigma|\epsilon_k + h\boldsymbol{m}\cdot\boldsymbol{\sigma}|k,\uparrow\rangle\, c^\dagger_{k,\sigma}c_{k,\uparrow} + \langle k,\sigma|\epsilon_k + h\boldsymbol{m}\cdot\boldsymbol{\sigma}|k,\downarrow\rangle\, c^\dagger_{k,\sigma}c_{k,\downarrow}\Big]\\
&= \sum_{k,\sigma}\Big[\langle k,\sigma|\epsilon_k + hm_z|k,\uparrow\rangle\, c^\dagger_{k,\sigma}c_{k,\uparrow} + \langle k,\sigma|h(m_x+\mathrm{i}m_y)|k,\downarrow\rangle\, c^\dagger_{k,\sigma}c_{k,\uparrow}\\
&\quad + \langle k,\sigma|\epsilon_k - hm_z|k,\downarrow\rangle\, c^\dagger_{k,\sigma}c_{k,\downarrow} + \langle k,\sigma|h(m_x-\mathrm{i}m_y)|k,\uparrow\rangle\, c^\dagger_{k,\sigma}c_{k,\downarrow}\Big]\\
&= \sum_k\Big[(\epsilon_k + hm_z)c^\dagger_{k,\uparrow}c_{k,\uparrow} + h(m_x+\mathrm{i}m_y)c^\dagger_{k,\downarrow}c_{k,\uparrow} + (\epsilon_k - hm_z)c^\dagger_{k,\downarrow}c_{k,\downarrow} + (m_x-\mathrm{i}m_y)c^\dagger_{k,\uparrow}c_{k,\downarrow}\Big]\\
&= \sum_k \begin{pmatrix}c^\dagger_{k,\uparrow} & c^\dagger_{k,\downarrow}\end{pmatrix}\begin{bmatrix}\epsilon_k + hm_z & h(m_x-\mathrm{i}m_y)\\ h(m_x+\mathrm{i}m_y) & \epsilon_k - hm_z\end{bmatrix}\begin{pmatrix}c_{k,\uparrow}\\c_{k,\downarrow}\end{pmatrix}
\end{aligned}$$

Where we have used that the states $|k,\sigma\rangle$ constitute an orthonormal basis. Commutation of the creation/annihilation operators produces a sign change and a constant energy term that we ignore, giving

$$\begin{aligned} H_F^h &= -\sum_k \left[(\epsilon_k + hm_z) c_{k,\uparrow} c_{k,\uparrow}^\dagger + h(m_x + \mathrm{i}m_y) c_{k,\uparrow} c_{k,\downarrow}^\dagger + (\epsilon_k - hm_z) c_{k,\downarrow} c_{k,\downarrow}^\dagger + (m_x - \mathrm{i}m_y) c_{k,\downarrow} c_{k,\uparrow}^\dagger \right] \\ &= \sum_k \begin{pmatrix} c_{k,\uparrow} & c_{k,\downarrow} \end{pmatrix} \begin{bmatrix} -\epsilon_k - hm_z & -h(m_x + \mathrm{i}m_y) \\ -h(m_x - \mathrm{i}m_y) & -\epsilon_k + hm_z \end{bmatrix} \begin{pmatrix} c_{k,\uparrow}^\dagger \\ c_{k,\downarrow}^\dagger \end{pmatrix} \end{aligned}$$

and we get for the whole system

$$H_{F,k} = \begin{bmatrix} \epsilon_k + hm_z & h(m_x - \mathrm{i}m_y) & 0 & 0 \\ h(m_x + \mathrm{i}m_y) & \epsilon_k - hm_z & 0 & 0 \\ 0 & 0 & -\epsilon_k - hm_z & -h(m_x + \mathrm{i}m_y) \\ 0 & 0 & -h(m_x - \mathrm{i}m_y) & -\epsilon_k + hm_z \end{bmatrix} \tag{5.10}$$

Solving for the (normalized) eigenvectors yields four states with energies $E = \pm\epsilon_k \pm h$ corresponding to electrons with spin parallel ($\uparrow$) or antiparallel ($\downarrow$) to the magnetization, and the holes resulting from removing these electrons.

$$\psi_{e\uparrow} = \frac{1}{\sqrt{2}} \begin{pmatrix} \sqrt{1+m_z} \\ \frac{m_x + \mathrm{i}m_y}{\sqrt{1+m_z}} \\ 0 \\ 0 \end{pmatrix} e^{\mathrm{i}k_{e\uparrow}x} \qquad \psi_{h\uparrow} = \frac{1}{\sqrt{2}} \begin{pmatrix} 0 \\ 0 \\ \sqrt{1+m_z} \\ \frac{m_x - \mathrm{i}m_y}{\sqrt{1+m_z}} \end{pmatrix} e^{\mathrm{i}k_{h\uparrow}x} \tag{5.11}$$

$$\psi_{e\downarrow} = \frac{1}{\sqrt{2}} \begin{pmatrix} \sqrt{1-m_z} \\ -\frac{m_x + \mathrm{i}m_y}{\sqrt{1-m_z}} \\ 0 \\ 0 \end{pmatrix} e^{\mathrm{i}k_{e\downarrow}x} \qquad \psi_{h\downarrow} = \frac{1}{\sqrt{2}} \begin{pmatrix} 0 \\ 0 \\ \sqrt{1-m_z} \\ -\frac{m_x - \mathrm{i}m_y}{\sqrt{1-m_z}} \end{pmatrix} e^{\mathrm{i}k_{h\downarrow}x} \tag{5.12}$$

The momenta are given by

$$k_{e\uparrow} = \frac{\sqrt{2m}}{\hbar}\left[\mu + E - h\right]^{1/2} = k_F\left[1 + \frac{E}{\mu} - \widetilde{h}\right]^{1/2} \qquad k_{h\uparrow} = \frac{\sqrt{2m}}{\hbar}\left[\mu - E - h\right]^{1/2} = k_F\left[1 - \frac{E}{\mu} - \widetilde{h}\right]^{1/2} \tag{5.13}$$

$$k_{e\downarrow} = \frac{\sqrt{2m}}{\hbar}\left[\mu + E + h\right]^{1/2} = k_F\left[1 + \frac{E}{\mu} + \widetilde{h}\right]^{1/2} \qquad k_{h\downarrow} = \frac{\sqrt{2m}}{\hbar}\left[\mu - E + h\right]^{1/2} = k_F\left[1 - \frac{E}{\mu} + \widetilde{h}\right]^{1/2} \tag{5.14}$$

where we have introduced the dimensionless energy parameter $\widetilde{h} = h/\mu$. Note that the use of arrows as subscripts here differs from our earlier use where it denoted spin relative to the z-axis. Going forward, to avoid ambiguity, this combination of e(h) and arrows will only be used for the ferromagnet where the arrows reference the magnetization direction.

5.2 Andreev bound state system

We now calculate the energies for Andreev bound states in the junction, allowing wave functions in the SOC and ferromagnet elements to be arbitrary combinations of eigenstates propagating in either direction. For the two superconductors, we allow only outgoing states which in the energy regime of Andreev bound states ($E^2 < \Delta^2$) correspond to wave functions with an exponential decay moving into the superconductors. At each interface we have a delta function potential barrier of strength V_0. We are left with 24 coefficients denoting the arbitrary weights of the allowed eigenstates, and we produce 12 equations (three 4-spinor equations) from demanding continuity of the wave function at each interface. By integrating over an infinitesimal distance across each interface we produce a further three spinor equations and are left with a system of 24 linear equations in 24 variables. We will not be interested in solving the system, but we will demand that the system must have a solution. Writing the system $A\boldsymbol{x} = 0$, where A is a 24-by-24 matrix and $\boldsymbol{x}$ is a vector containing the 24 coefficients, we demand $\mathrm{Det}A = 0$. This will allow us to scale any of the coefficients without affecting our results.

For the left (L) and rigth (R) superconductors we then have

$$\psi_L = \left[a_L \begin{pmatrix} e^{i\beta} \\ 0 \\ 0 \\ e^{-i\phi_L} \end{pmatrix} + b_L \begin{pmatrix} 0 \\ e^{i\beta} \\ -e^{-i\phi_L} \\ 0 \end{pmatrix} \right] e^{-ik^+ x} \quad + \quad \left[c_L \begin{pmatrix} e^{-i\beta} \\ 0 \\ 0 \\ e^{-i\phi_L} \end{pmatrix} + d_L \begin{pmatrix} 0 \\ e^{-i\beta} \\ -e^{-i\phi_L} \\ 0 \end{pmatrix} \right] e^{ik^- x} \tag{5.15}$$

$$\psi_R = \left[a_R \begin{pmatrix} e^{i\beta} \\ 0 \\ 0 \\ e^{-i\phi_R} \end{pmatrix} + b_R \begin{pmatrix} 0 \\ e^{i\beta} \\ -e^{-i\phi_R} \\ 0 \end{pmatrix} \right] e^{ik^+ x} \quad + \quad \left[c_R \begin{pmatrix} e^{-i\beta} \\ 0 \\ 0 \\ e^{-i\phi_R} \end{pmatrix} + d_R \begin{pmatrix} 0 \\ e^{-i\beta} \\ -e^{-i\phi_R} \\ 0 \end{pmatrix} \right] e^{-ik^- x} \tag{5.16}$$

where we have simplified the spinors by introducing a new variable $e^{i\beta} = u_k/v_k$ and absorbing one of the coherence factors into each coefficient.

For the ferromagnet, we have eight contributions to the wave function. Absorbing a factor $\sqrt{\frac{2}{1\pm m_z}}$ into the coefficients gives

$$\begin{aligned}\psi_F = {} & e^+_\uparrow \begin{pmatrix} 1+m_z \\ m_x+\mathrm{i}m_y \\ 0 \\ 0 \end{pmatrix} e^{\mathrm{i}k_{e\uparrow}x} + e^-_\uparrow \begin{pmatrix} 1+m_z \\ m_x+\mathrm{i}m_y \\ 0 \\ 0 \end{pmatrix} e^{-\mathrm{i}k_{e\uparrow}x} + e^+_\downarrow \begin{pmatrix} 1-m_z \\ -(m_x+\mathrm{i}m_y) \\ 0 \\ 0 \end{pmatrix} e^{\mathrm{i}k_{e\downarrow}x} \\ & + e^-_\downarrow \begin{pmatrix} 1-m_z \\ -(m_x+\mathrm{i}m_y) \\ 0 \\ 0 \end{pmatrix} e^{-\mathrm{i}k_{e\downarrow}x} + h^+_\uparrow \begin{pmatrix} 0 \\ 0 \\ 1+m_z \\ m_x-\mathrm{i}m_y \end{pmatrix} e^{\mathrm{i}k_{h\uparrow}x} + h^-_\uparrow \begin{pmatrix} 0 \\ 0 \\ 1+m_z \\ m_x-\mathrm{i}m_y \end{pmatrix} e^{-\mathrm{i}k_{h\uparrow}x} \\ & + h^+_\downarrow \begin{pmatrix} 0 \\ 0 \\ 1-m_z \\ -(m_x-\mathrm{i}m_y) \end{pmatrix} e^{\mathrm{i}k_{h\downarrow}x} + h^-_\downarrow \begin{pmatrix} 0 \\ 0 \\ 1-m_z \\ -(m_x-\mathrm{i}m_y) \end{pmatrix} e^{-\mathrm{i}k_{h\downarrow}x}\end{aligned}$$

Finally, the SOC element has the wave function

$$\begin{aligned}\psi_{SOC} = {} & a^+ \begin{pmatrix} 1 \\ 0 \\ 0 \\ 0 \end{pmatrix} e^{\mathrm{i}k_1 x} + b^+ \begin{pmatrix} 0 \\ 1 \\ 0 \\ 0 \end{pmatrix} e^{\mathrm{i}k_2 x} + c^+ \begin{pmatrix} 0 \\ 0 \\ 1 \\ 0 \end{pmatrix} e^{\mathrm{i}k_3 x} + d^+ \begin{pmatrix} 0 \\ 0 \\ 0 \\ 1 \end{pmatrix} e^{\mathrm{i}k_4 x} \\ & + a^- \begin{pmatrix} 1 \\ 0 \\ 0 \\ 0 \end{pmatrix} e^{-\mathrm{i}k_2 x} + b^- \begin{pmatrix} 0 \\ 1 \\ 0 \\ 0 \end{pmatrix} e^{-\mathrm{i}k_1 x} + c^- \begin{pmatrix} 0 \\ 0 \\ 1 \\ 0 \end{pmatrix} e^{-\mathrm{i}k_4 x} + d^- \begin{pmatrix} 0 \\ 0 \\ 0 \\ 1 \end{pmatrix} e^{-\mathrm{i}k_3 x}\end{aligned}$$

Taking the interface between the SOC and ferromagnetic elements to be at $x = 0$, we let the lengths of the SOC element and the ferromagnet be x_1 and x_2, respectively. The continuity condition at each interface then reads

$$\psi_L(-x_1) = \psi_{SOC}(-x_1) \qquad \psi_{SOC}(0) = \psi_F(0) \qquad \psi_F(x_2) = \psi_R(x_2) \tag{5.17}$$

Writing them all out on homogeneous form, the first condition gives the equations for rows 1 through 4 of our matrix A:

$$0 = -\begin{pmatrix} a^+ \\ 0 \\ 0 \\ 0 \end{pmatrix} e^{-\mathrm{i}k_1 x_1} - \begin{pmatrix} a^- \\ 0 \\ 0 \\ 0 \end{pmatrix} e^{\mathrm{i}k_2 x_1} - \begin{pmatrix} 0 \\ b^+ \\ 0 \\ 0 \end{pmatrix} e^{-\mathrm{i}k_2 x_1} - \begin{pmatrix} 0 \\ b^- \\ 0 \\ 0 \end{pmatrix} e^{\mathrm{i}k_1 x_1} - \begin{pmatrix} 0 \\ 0 \\ c^+ \\ 0 \end{pmatrix} e^{-\mathrm{i}k_3 x_1} - \begin{pmatrix} 0 \\ 0 \\ c^- \\ 0 \end{pmatrix} e^{\mathrm{i}k_4 x_1}$$
$$- \begin{pmatrix} 0 \\ 0 \\ 0 \\ d^+ \end{pmatrix} e^{-\mathrm{i}k_4 x_1} - \begin{pmatrix} 0 \\ 0 \\ 0 \\ d^- \end{pmatrix} e^{\mathrm{i}k_3 x_1} + \begin{pmatrix} a_L e^{\mathrm{i}\beta} \\ b_L e^{\mathrm{i}\beta} \\ -b_L e^{-\mathrm{i}\phi_L} \\ a_L e^{-\mathrm{i}\phi_L} \end{pmatrix} e^{\mathrm{i}k^+ x_1} + \begin{pmatrix} c_L e^{-\mathrm{i}\beta} \\ d_L e^{-\mathrm{i}\beta} \\ -d_L e^{-\mathrm{i}\phi_L} \\ c_L e^{-\mathrm{i}\phi_L} \end{pmatrix} e^{-\mathrm{i}k^- x_1}$$

The second condition determines rows 5 through 8:

$$0 = \begin{pmatrix} a^+ + a^- \\ b^+ + b^- \\ c^+ + c^- \\ d^+ + d^- \end{pmatrix} - \left[e_\uparrow^+ + e_\uparrow^-\right] \begin{pmatrix} 1 + m_z \\ m_x + \mathrm{i}m_y \\ 0 \\ 0 \end{pmatrix} - \left[e_\downarrow^+ + e_\downarrow^-\right] \begin{pmatrix} 1 - m_z \\ -(m_x + \mathrm{i}m_y) \\ 0 \\ 0 \end{pmatrix}$$
$$- \left[h_\uparrow^+ + h_\uparrow^-\right] \begin{pmatrix} 0 \\ 0 \\ 1 + m_z \\ m_x - \mathrm{i}m_y \end{pmatrix} - \left[h_\downarrow^+ + h_\downarrow^-\right] \begin{pmatrix} 0 \\ 0 \\ 1 - m_z \\ \mathrm{i}m_y - m_x \end{pmatrix}$$

And rows 9 through 12 are given by the third condition:

$$0 = e_\uparrow^+ \begin{pmatrix} 1 + m_z \\ m_x + \mathrm{i}m_y \\ 0 \\ 0 \end{pmatrix} e^{\mathrm{i}k_{e\uparrow} x_2} + e_\uparrow^- \begin{pmatrix} 1 + m_z \\ m_x + \mathrm{i}m_y \\ 0 \\ 0 \end{pmatrix} e^{-\mathrm{i}k_{e\uparrow} x_2} + e_\downarrow^+ \begin{pmatrix} 1 - m_z \\ -(m_x + \mathrm{i}m_y) \\ 0 \\ 0 \end{pmatrix} e^{\mathrm{i}k_{e\downarrow} x_2}$$
$$+ e_\downarrow^- \begin{pmatrix} 1 - m_z \\ -(m_x + \mathrm{i}m_y) \\ 0 \\ 0 \end{pmatrix} e^{-\mathrm{i}k_{e\downarrow} x_2} + h_\uparrow^+ \begin{pmatrix} 0 \\ 0 \\ 1 + m_z \\ m_x - \mathrm{i}m_y \end{pmatrix} e^{\mathrm{i}k_{h\uparrow} x_2} + h_\uparrow^- \begin{pmatrix} 0 \\ 0 \\ 1 + m_z \\ m_x - \mathrm{i}m_y \end{pmatrix} e^{-\mathrm{i}k_{h\uparrow} x_2}$$
$$+ h_\downarrow^+ \begin{pmatrix} 0 \\ 0 \\ 1 - m_z \\ \mathrm{i}m_y - m_x \end{pmatrix} e^{\mathrm{i}k_{h\downarrow} x_2} + h_\downarrow^- \begin{pmatrix} 0 \\ 0 \\ 1 - m_z \\ \mathrm{i}m_y - m_x \end{pmatrix} e^{-\mathrm{i}k_{h\downarrow} x_2} + \begin{pmatrix} -a_R e^{\mathrm{i}\beta} \\ -b_R e^{\mathrm{i}\beta} \\ b_R e^{-\mathrm{i}\phi_R} \\ -a_R e^{-\mathrm{i}\phi_R} \end{pmatrix} e^{\mathrm{i}k^+ x_2} + \begin{pmatrix} -c_R e^{-\mathrm{i}\beta} \\ -d_R e^{-\mathrm{i}\beta} \\ d_R e^{-\mathrm{i}\phi_R} \\ -c_R e^{-\mathrm{i}\phi_R} \end{pmatrix} e^{-\mathrm{i}k^- x_2}$$

With the potential $V(x) = V_0\left[\delta(-x_1)+\delta(0)+\delta(x_2)\right]\mathrm{diag}\left(1,1,-1,-1\right)$ the Schrödinger

equation of the system is $\big[H+V(x)\big]\psi = E\psi$. Integrating over an infinitesimal distance η across our interfaces leaves only terms with a delta function and terms with derivatives of the wavefunction with regards to x. Thus all our Hamiltonian matrices reduce to $\frac{\hbar^2}{2m}\mathrm{diag}\big(-\frac{\partial^2}{\partial x^2}, -\frac{\partial^2}{\partial x^2}, \frac{\partial^2}{\partial x^2}, \frac{\partial^2}{\partial x^2}\big)$ (since $\epsilon_k = \frac{\hbar^2 k^2}{2m} - \mu$ and the operator form of k is $-\mathrm{i}\frac{\partial}{\partial x}$). For the interface at $-x_1$ we are left with

$$\lim_{\eta\to 0}\int_{-x_1-\eta}^{-x_1+\eta}\Big[\frac{\hbar^2}{2m}\psi'' - V(x)\psi\Big]\mathrm{d}x = \frac{\hbar^2}{2m}\big[\psi'(-x_1^+) - \psi'(-x_1^-)\big] - V_0\psi(-x_1) = 0 \quad (5.18)$$

where we have used that $\int_{0^-}^{0^+} f''(x)\mathrm{d}x = f'(0^+) - f'(0^-)$. As $x = -x_1^+$ is in the SOC element and $x = -x_1^-$ is in the left superconductor, we have

$$\psi'_{SOC}(-x_1) - \psi'_L(-x_1) = \frac{2mV_0}{\hbar^2}\psi_L(-x_1) \quad (5.19)$$

$$0 = \frac{1}{\mathrm{i}k_F}\big[\psi'_{SOC}(-x_1) - \psi'_L(-x_1)\big] + \mathrm{i}Z\psi_L(-x_1) \quad (5.20)$$

where we have introduced the barrier strength parameter $Z = \frac{2mV_0}{\hbar^2 k_F}$ for convenience. In the same way, we get for the other interfaces

$$0 = \frac{1}{\mathrm{i}k_F}\big[\psi'_F(0) - \psi'_{SOC}(0)\big] + \mathrm{i}Z\psi_{SOC}(0) \quad (5.21)$$

$$0 = \frac{1}{\mathrm{i}k_F}\big[\psi'_R(x_2) - \psi'_F(x_2)\big] + \mathrm{i}Z\psi_R(x_2) \quad (5.22)$$

Inserting our spinor wave functions into (5.20) gives us, for rows 13 through 16 of A:

$$
\begin{aligned}
0 = &\frac{k_1}{k_F}\begin{pmatrix} a^+ \\ 0 \\ 0 \\ 0 \end{pmatrix} e^{-\mathrm{i}k_1 x_1} - \frac{k_2}{k_F}\begin{pmatrix} a^- \\ 0 \\ 0 \\ 0 \end{pmatrix} e^{\mathrm{i}k_2 x_1} + \frac{k_2}{k_F}\begin{pmatrix} 0 \\ b^+ \\ 0 \\ 0 \end{pmatrix} e^{-\mathrm{i}k_2 x_1} - \frac{k_1}{k_F}\begin{pmatrix} 0 \\ b^- \\ 0 \\ 0 \end{pmatrix} e^{\mathrm{i}k_1 x_1} \\
&+ \frac{k_3}{k_F}\begin{pmatrix} 0 \\ 0 \\ c^+ \\ 0 \end{pmatrix} e^{-\mathrm{i}k_3 x_1} - \frac{k_4}{k_F}\begin{pmatrix} 0 \\ 0 \\ c^- \\ 0 \end{pmatrix} e^{\mathrm{i}k_4 x_1} + \frac{k_4}{k_F}\begin{pmatrix} 0 \\ 0 \\ 0 \\ d^+ \end{pmatrix} e^{-\mathrm{i}k_4 x_1} - \frac{k_3}{k_F}\begin{pmatrix} 0 \\ 0 \\ 0 \\ d^- \end{pmatrix} e^{\mathrm{i}k_3 x_1} \\
&+ \left(\mathrm{i}Z + \frac{k^+}{k_F}\right)\begin{pmatrix} a_L e^{\mathrm{i}\beta} \\ b_L e^{\mathrm{i}\beta} \\ -b_L e^{-\mathrm{i}\phi_L} \\ a_L e^{-\mathrm{i}\phi_L} \end{pmatrix} e^{\mathrm{i}k^+ x_1} + \left(\mathrm{i}Z - \frac{k^-}{k_F}\right)\begin{pmatrix} c_L e^{-\mathrm{i}\beta} \\ d_L e^{-\mathrm{i}\beta} \\ -d_L e^{-\mathrm{i}\phi_L} \\ c_L e^{-\mathrm{i}\phi_L} \end{pmatrix} e^{-\mathrm{i}k^- x_1}
\end{aligned}
$$

Writing out (5.21) produces the equations for rows 17 through 20:

$$
\begin{aligned}
0 = &\left(\mathrm{i}Z - \frac{k_1}{k_F}\right)\begin{pmatrix} a^+ \\ 0 \\ 0 \\ 0 \end{pmatrix} + \left(\mathrm{i}Z + \frac{k_2}{k_F}\right)\begin{pmatrix} a^- \\ 0 \\ 0 \\ 0 \end{pmatrix} + \left(\mathrm{i}Z - \frac{k_2}{k_F}\right)\begin{pmatrix} 0 \\ b^+ \\ 0 \\ 0 \end{pmatrix} + \left(\mathrm{i}Z + \frac{k_1}{k_F}\right)\begin{pmatrix} 0 \\ b^- \\ 0 \\ 0 \end{pmatrix} \\
&+ \left(\mathrm{i}Z - \frac{k_3}{k_F}\right)\begin{pmatrix} 0 \\ 0 \\ c^+ \\ 0 \end{pmatrix} + \left(\mathrm{i}Z + \frac{k_4}{k_F}\right)\begin{pmatrix} 0 \\ 0 \\ c^- \\ 0 \end{pmatrix} + \left(\mathrm{i}Z - \frac{k_4}{k_F}\right)\begin{pmatrix} 0 \\ 0 \\ 0 \\ d^+ \end{pmatrix} + \left(\mathrm{i}Z + \frac{k_3}{k_F}\right)\begin{pmatrix} 0 \\ 0 \\ 0 \\ d^- \end{pmatrix} \\
&+ \left[e_\uparrow^+ - e_\uparrow^-\right]\frac{k_{e\uparrow}}{k_F}\begin{pmatrix} 1+m_z \\ m_x + \mathrm{i}m_y \\ 0 \\ 0 \end{pmatrix} + \left[e_\downarrow^+ - e_\downarrow^-\right]\frac{k_{e\downarrow}}{k_F}\begin{pmatrix} 1-m_z \\ -(m_x + \mathrm{i}m_y) \\ 0 \\ 0 \end{pmatrix} \\
&+ \left[h_\uparrow^+ - h_\uparrow^-\right]\frac{k_{h\uparrow}}{k_F}\begin{pmatrix} 0 \\ 0 \\ 1+m_z \\ m_x - \mathrm{i}m_y \end{pmatrix} + \left[h_\downarrow^+ - h_\downarrow^-\right]\frac{k_{h\downarrow}}{k_F}\begin{pmatrix} 0 \\ 0 \\ 1-m_z \\ \mathrm{i}m_y - m_x \end{pmatrix}
\end{aligned}
$$

And finally, (5.22) fills in the final rows, 21 through 24:

$$
\begin{aligned}
0 = &-e_\uparrow^+ \frac{k_{e\uparrow}}{k_F}\begin{pmatrix}1+m_z\\ m_x+\mathrm{i}m_y\\ 0\\ 0\end{pmatrix} e^{\mathrm{i}k_{e\uparrow}x_2} + e_\uparrow^- \frac{k_{e\uparrow}}{k_F}\begin{pmatrix}1+m_z\\ m_x+\mathrm{i}m_y\\ 0\\ 0\end{pmatrix} e^{-\mathrm{i}k_{e\uparrow}x_2} - e_\downarrow^+ \frac{k_{e\downarrow}}{k_F}\begin{pmatrix}1-m_z\\ -(m_x+\mathrm{i}m_y)\\ 0\\ 0\end{pmatrix} e^{\mathrm{i}k_{e\downarrow}x_2}\\
&+ e_\downarrow^- \frac{k_{e\downarrow}}{k_F}\begin{pmatrix}1-m_z\\ -(m_x+\mathrm{i}m_y)\\ 0\\ 0\end{pmatrix} e^{-\mathrm{i}k_{e\downarrow}x_2} - h_\uparrow^+ \frac{k_{h\uparrow}}{k_F}\begin{pmatrix}0\\ 0\\ 1+m_z\\ m_x-\mathrm{i}m_y\end{pmatrix} e^{\mathrm{i}k_{h\uparrow}x_2} + h_\uparrow^- \frac{k_{h\uparrow}}{k_F}\begin{pmatrix}0\\ 0\\ 1+m_z\\ m_x-\mathrm{i}m_y\end{pmatrix} e^{-\mathrm{i}k_{h\uparrow}x_2}\\
&- h_\downarrow^+ \frac{k_{h\downarrow}}{k_F}\begin{pmatrix}0\\ 0\\ 1-m_z\\ \mathrm{i}m_y-m_x\end{pmatrix} e^{\mathrm{i}k_{h\downarrow}x_2} + h_\downarrow^- \frac{k_{h\downarrow}}{k_F}\begin{pmatrix}0\\ 0\\ 1-m_z\\ \mathrm{i}m_y-m_x\end{pmatrix} e^{-\mathrm{i}k_{h\downarrow}x_2}\\
&+ \left(\mathrm{i}Z+\frac{k^+}{k_F}\right)\begin{pmatrix}a_R e^{\mathrm{i}\beta}\\ b_R e^{\mathrm{i}\beta}\\ -b_R e^{-\mathrm{i}\phi_R}\\ a_R e^{-\mathrm{i}\phi_R}\end{pmatrix} e^{\mathrm{i}k^+x_2} + \left(\mathrm{i}Z-\frac{k^-}{k_F}\right)\begin{pmatrix}c_R e^{-\mathrm{i}\beta}\\ d_R e^{-\mathrm{i}\beta}\\ -d_R e^{-\mathrm{i}\phi_R}\\ c_R e^{-\mathrm{i}\phi_R}\end{pmatrix} e^{-\mathrm{i}k^-x_2}
\end{aligned}
$$

We note that as the wave functions of the superconductors are evaluated at only one position, each of the exponential factors are always paired with the same coefficient and can thus be absorbed. We introduce $\widetilde{a}_L = a_L e^{\mathrm{i}k^+x_1}$, $\widetilde{a}_R = a_R e^{\mathrm{i}k^+x_2}$ and so on, and define our variable vector as

$$
\boldsymbol{x} = (a^+, a^-, b^+, b^-, c^+, c^-, d^+, d^-, e_\uparrow^+, e_\uparrow^-, e_\downarrow^+, e_\downarrow^-, h_\uparrow^+, h_\uparrow^-, h_\downarrow^+, h_\downarrow^-, \widetilde{a}_L, \widetilde{b}_L, \widetilde{c}_L, \widetilde{d}_L, \widetilde{a}_R, \widetilde{b}_R, \widetilde{c}_R, \widetilde{d}_R)^T
$$

yielding the matrix seen in Figures 5.2 and 5.3 (split in two parts for readability) as a description of our linear system. In principle, one could calculate the determinant analytically and $\mathrm{Det}A = 0$ would give us an equation for β and thus for the allowed energies, since

$$
e^{\mathrm{i}\beta} = \frac{u}{v} = \left[\frac{E+\sqrt{E^2-\Delta^2}}{E-\sqrt{E^2-\Delta^2}}\right]^{1/2} = \left[2\frac{E^2}{\Delta^2} + 2\frac{E}{\Delta}\sqrt{\frac{E^2}{\Delta^2}-1} - 1\right]^{1/2} = \frac{E}{\Delta} + \sqrt{\frac{E^2}{\Delta^2}-1} \tag{5.23}
$$

so that

$$
\beta = -\mathrm{i}\ln\left(\frac{E}{\Delta} + \sqrt{\frac{E^2}{\Delta^2}-1}\right) = \arccos\frac{E}{\Delta} \tag{5.24}
$$

which we can verify by inserting our expression for β in $\cos(\beta) = \frac{1}{2}\left[e^{i\beta} + e^{-i\beta}\right] = \frac{E}{\Delta}$. However, various attempted approximation schemes failed to render the equation humanly legible, and instead a numerical approach was adopted.

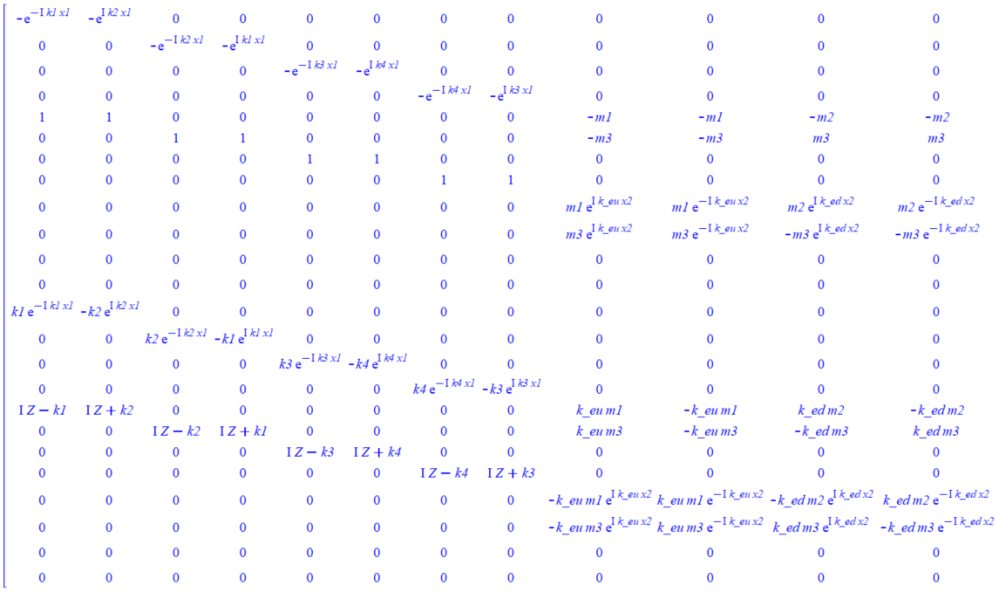

Figure 5.2: Part one of the matrix describing our linear system. See caption of Figure 5.3.

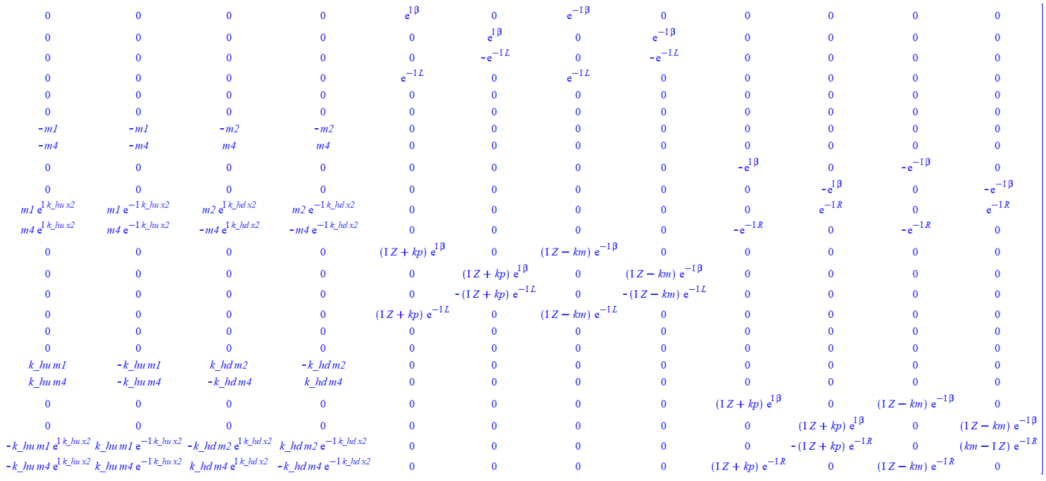

Figure 5.3: Part two of the matrix describing our linear system. For readability we have used the following shorthand notations: $m1 = 1 + m_z, m2 = 1 - m_z, m3 = m_x + im_y, m4 = m_x - im_y, L = \phi_L, R = \phi_R$. All momenta are given in units of k_F, i.e. $kp = \frac{k^+}{k_F}, km = \frac{k^-}{k_F}$, $k\_eu = \frac{k_{e\uparrow}}{k_F}$, $k\_hd = \frac{k_{h\downarrow}}{k_F}$ etc. The positions are given in units of $1/k_F$ ($x1 = x_1 k_F$, $x2 = x_2 k_F$) and lastly the imaginary unit is denoted by a capitalized letter 'I'.

6. Numerical methods

With appropriate values for the various parameters, we can quickly calculate the numerical value of the determinant of our matrix. If we hold all other parameters constant while changing the energy, we can find the energies for which the value of the determinant (within numerical rounding errors) goes to zero. These energies E_i, we will interpret as the energy levels of a fermionic system. For the thermodynamic properties of a system of fermions without conservation of particle number, we will be interested in the fermionic grand partition function (found in e.g. [41]):

$$\mathcal{Z} = \prod_i \left(1 + e^{-\frac{E_i}{k_B T}}\right) \tag{6.1}$$

giving the free energy of the system as

$$F = -k_B T \ln \mathcal{Z} = -k_B T \sum_i \ln\left(1 + e^{-\frac{E_i}{k_B T}}\right) \tag{6.2}$$

where k_B, T denotes the Boltzmann constant and the temperature, respectively. In general, the (supercurrent dependent) free energy of a Josephson junction is given as an integral over the supercurrent [42]

$$F(\Delta\phi) = \frac{\hbar}{2e} \int_0^{\Delta\phi} J(\phi') \mathrm{d}\phi' \tag{6.3}$$

where we for the moment do not write out explicitly the dependence of parameters other than the phase. Although junctions similar to ours (e.g. with a single non-superconducting element that is both magnetic and exhibits Rashba SOC) can be used to create ϕ_0-junctions [43], we will assume our system does not constitute such a junction, unless our calculations produce a shifted ground state or a current at $\Delta\phi = 0$. Under this assumption, the sine series general expression for the Josephson current from Chapter 2 holds, and we can thus expect the free energy to be given by a series of cosines:

$$F(\Delta\phi) = F_{\text{other}} + \sum_{n=1}^{\infty} \frac{\hbar J_n}{2e} \frac{1 - \cos(n\Delta\phi)}{n} = \sum_{n=0}^{\infty} F_n \cos(n\Delta\phi) \tag{6.4}$$

where F_{other} is a constant (wrt. phase) containing contributions to free energy not dependent on the supercurrent. In the last equality, we absorb all constant terms (wrt. phase) into F_0. Considering again parameters other than phase, we expect the coefficients F_n to exhibit a dependence on e.g. the magnetization direction of the ferromagnet.

Whatever the form of the free energy, following the effective field formalism of Chapter 3, we would like to solve for the effective field due to the Andreev bound state current in the junction:

$$\boldsymbol{H}_{\text{ABS}} = -\frac{\delta U_{\text{ABS}}[\boldsymbol{M}]}{\delta \boldsymbol{M}} = -\frac{\partial U_{\text{ABS}}(\boldsymbol{M})}{\partial \boldsymbol{M}} = -\frac{1}{V}\frac{\partial F_{\text{ABS}}}{\partial \boldsymbol{M}} \tag{6.5}$$

where the second equality holds in our approximation of the ferromagnet as a single magnetic domain, and we identify the relevant energy density as the free energy density of the Andreev bound state system in the ferromagnet $U_{\text{ABS}} = \frac{F_{\text{ABS}}}{V}$ where V is the volume of the ferromagnet. Though it might naïvely seem that F_{ABS} is exactly the free energy we have calculated, F, the relationship between the two energies is not quite that simple. Additionally, it is not obvious whether the effective fields of Chapter 3, which are based on energy densities, are directly applicable to our essentially two-dimensional ferromagnet. These concerns have been relegated to our discussion in Chapter 8, and for now we use the formalism from Chapter 3 (essentially disregarding the fact that our magnet is a thin plate in the S-F-S cases discussed below). With regards to the energy density, we proceed on the assumption that the correct energy F_{ABS} is proportional to our F, so that the dimensionless effective field is (in SI units):

$$\boldsymbol{h}_{\text{ABS}} = -C\frac{\partial F}{\partial \boldsymbol{m}} \qquad \text{where} \qquad C = \frac{1}{V}\frac{F_{\text{ABS}}}{F}\frac{1}{\mu_0 M_s^2} \tag{6.6}$$

and $C > 0$ has units inverse energy as we should expect.

6.1 Energy calculations

Other parameters held constant, choosing an energy in the ABS regime ($-\Delta \leq E \leq \Delta$) sets the values of β and the various momenta and thus allows calculation of the numerical value of the determinant. In Figure 6.1 the determinant value is plotted for the possible ABS energies, and the MATLAB inbuilt function "findpeaks" has been used to identify the energies that give $\text{Det}A = 0$.

Some care must be taken using this method, as two energies that become degenerate under parameter variation will suddenly register as one energy level, potentially creating discontinuities in the calculated free energy. A solution to this problem is to encode an expectation of the number of allowed energies such that,

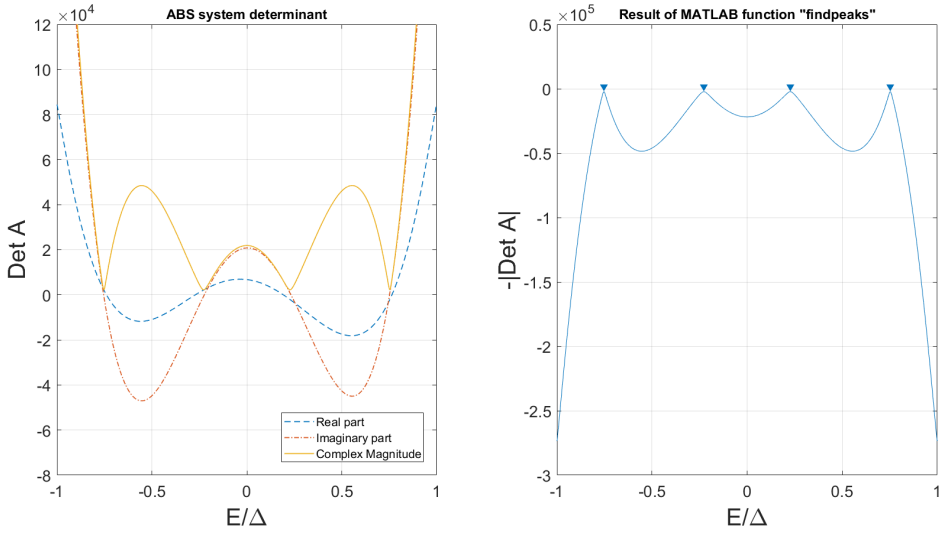

Figure 6.1: Plot of determinant of Andreev bound state system as a function of energy and a depiction of how the MATLAB "findpeaks" function is used to identify the permissible energies by finding the zeros of the determinant. These plots were made using a somewhat arbitrarily chosen set of parameters, and are meant only to illustrate the methods used. ($\Delta\phi = 4\pi/5$, $\theta_m = \pi/3$, $\phi_m = \pi/3$, $\mu = 1$ eV, $\widetilde{\Delta} = 0.001$, $\widetilde{\alpha} = 0.1$, $\widetilde{h} = 0.05$, $Z = 0.5$, $x_1 k_F = 20$ and $x_2 k_F = 20$.)

for instance, two zeros found by "findpeaks" are interpreted as two two-fold degenerate energies. Additionally, the function is liable to find false zeros at the edges of the plot (i.e. at $E = \pm\Delta$) that must be removed. An expectation of four energy levels is used in the following and assumed to be successful if there are no discontinuities in the free energy. Varying $\Delta\phi = \phi_L - \phi_R$ while keeping the other parameters as in Figure 6.1 allows us to plot the Andreev energies (i.e. the zeros of the determinant) as functions of superconducting phase, producing the plot in Figure 6.2.

We note that in the regions where two of the energies approach zero, they become indistinguishable to our numerical scheme and are thus interpreted as a degenerate energy level at $E = 0$. Presumably, in the absence of numerical errors, the two branches would smoothly approach zero and meet in a single point on the $\Delta\phi$-axis rather than in an interval. As an estimation of the maximum error in free energy produced by this mechanism, we set $\Delta = 10 k_B T$ and calculate the change in free energy at each side of the interval when changing the middle energy branches from $\pm 0.05\Delta$ to zero. The change from $F(\pm 0.05\Delta, \pm 0.8\Delta)$ is -0.0062Δ, while the change from $F(\pm 0.05\Delta, \pm 0.9\Delta)$ is about -0.0061Δ. Thus, for the affected phase values we will be liable to underestimate the free energy by up to about half a percent of the gap energy.

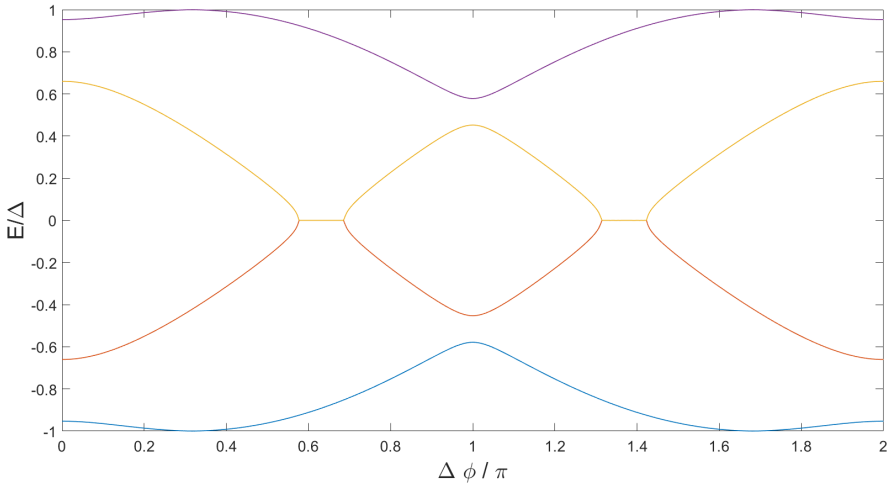

Figure 6.2: Plot of Andreev bound state energies as a function of superconducting phase $\Delta\phi = \phi_L - \phi_R$. Parameters are the same as in Figure 6.1 except for the variation of $\Delta\phi$. Notice that in the two regions where the two middle branches are close to zero, the two energies can no longer be distinguished and are treated as a degenerate energy level with value zero.

6.2 Validation of the numerical scheme

One strategy for assessing the validity of our model is to adjust our parameters so as to represent junctions for which there exists results that we should be able to reproduce. The simplest such case is the S-N-S junction with transparent interfaces (i.e. $Z = 0$), for which the supercurrent can be given as [44]:

$$J(\Delta\phi) = J_0 \sin\left(\frac{\Delta\phi}{2}\right) \tanh\left[\frac{\Delta}{2k_B T}\cos\left(\frac{\Delta\phi}{2}\right)\right] \tag{6.7}$$

which for $\Delta = 10k_B T$ gives a free energy of

$$F_{\mathrm{SNS}}(\Delta\phi) = \frac{\hbar}{2e}\int_0^{\Delta\phi} J(\phi')\mathrm{d}\phi' = F_0 \ln\left(\frac{\cosh(5)}{\cosh(5\cos(\Delta\phi/2))}\right) \tag{6.8}$$

where the zero point for the energy is implicitly set at $\Delta\phi = 0$ and the energy maximum is attained for $\Delta\phi = \pi$. We can produce numerical results for an S-N-S junction with our numerical scheme by setting the length of the SOC element and the exchange field strength to zero. As we are interested mainly in the functional dependence on phase, we circumvent the issue of determining the size of F_0 by a simple normalization: we divide both the analytical expression and our numerical results on the value they attain for $\Delta\phi = \pi$. The resulting expression for the free energy is plotted together with normalized numerical results in Figure 6.3. The nu-

merical results are in excellent agreement with the analytical expression.

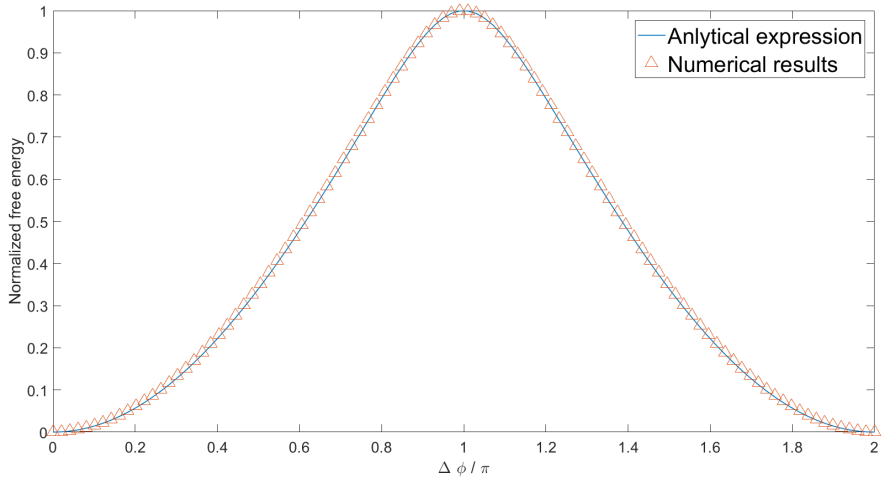

Figure 6.3: Comparison of numerical results and analytical expression (eq. (6.8)) for the free energy of a S-N-S junction. For the numerical results in this plot $\mu = 1$ eV, $\widetilde{h} = 0$, $\widetilde{\Delta} = 0.001$, $Z = 0$, $x_1 k_F = 0$ and $x_2 k_F = 20$.

As a further test of the numerical method, we attempt to reproduce the Andreev energy levels found for an S-F-S junction by Annunziata et al. [45] (in the case of pure Stoner magnetism). Setting the length of our SOC element to zero takes us to the S-F-S case, except that we are left with two barriers at the S-F interface, or equivalently, one barrier of double strength. Setting the remaining parameters to match the calculation of Andreev energies by Annunziata et al. (the right plot in Figure 6.4), and correcting for the double counting of barriers we produce the left plot in Figure 6.4. Several versions of this calculation was performed with randomized magnetization direction to verify that the reduced system is isotropic in spin space. No deviations from the results in Figure 6.4 were observed. The two sets of results are in excellent agreement, indicating that our numerical scheme reduces correctly to the S-F-S case.

Another characteristic of the S-F-S junction worth reproducing is the so called π-junction: a configuration for which the S-F-S junction energy minima occurs at $\Delta\phi = \pi$ instead of $\Delta\phi = 0$ as in the conventional junction [46, 47]. Note that this does not constitute a ϕ_0-junction: a phase shift of π in the free energy (and thus in the current) can be taken out of any term in a sine series: $\sin n(\Delta\phi + \pi) = \pm \sin n\Delta\phi$, producing a sign change for odd n. Thus we are left with zero current when there is no phase difference. For the simple (first order) sine current of the conventional Josephson junction $J(\Delta\phi) = J_0 \sin(\Delta\phi)$, the π-junction can be seen as a re-

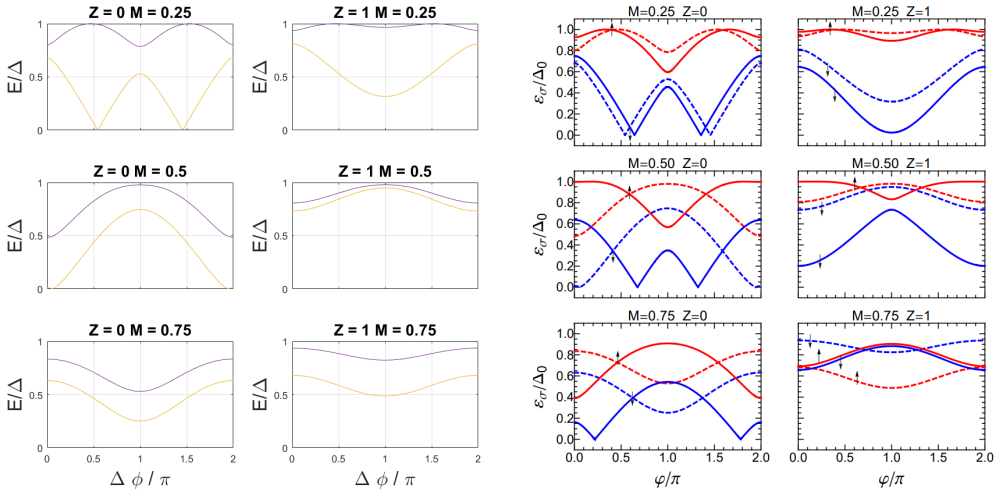

Figure 6.4: Plot of Andreev bound state energies as a function of superconducting phase $\Delta\phi = \phi_L - \phi_R$ for parameters $x_2 k_F = 10, \mu = 5\text{eV}, \Delta = 1\text{meV}$. Z is the barrier strength parameter and M determines the strength of the exchange field by $\widetilde{h} = 2M/(1+M^2)$. The right plot is from a treatment of Andreev states in S-F-S junctions by Annunziata et al. [45] and the dashed lines correspond to our system. The left plot results from setting the length of the SOC element to zero and correcting for double counting the barrier strength.

sult of a sign change in the current amplitude, $J_0 \rightarrow -J_0$. Such a change of the current amplitude has been predicted to occur with variations in both exchange field strength [46] and thickness [48] of the ferromagnetic element. In an attempt to reproduce these transitions, free energy has been calculated for select values for both exchange field strength and ferromagnet thickness, and the results are plotted in Figure 6.5. Variation of both parameters is seen to take the system from a normal junction to a π-junction, and interestingly, both transitions display a non-sinusoidal phase dependence for the free energy in the intermediate stage of the transition. We can understand this by noting that as the amplitude of the first order sine term changes smoothly from a positive to a negative value, it will be close to zero in some interval, and we will be left with the higher order terms that would normally be small compared to the first order term.

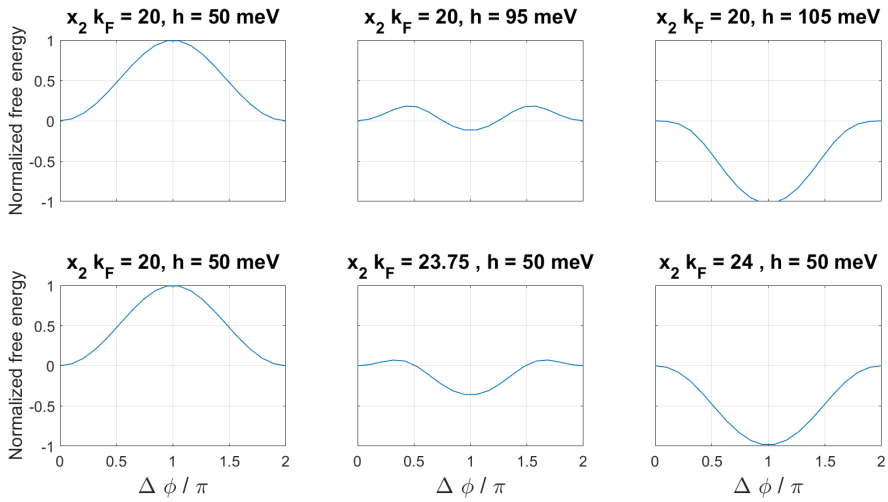

Figure 6.5: Normalized free energy plotted as a function of phase for various values for exchange field strength h and ferromagnet thickness x_2. For each configuration the zero point energy is defined as the energy at zero phase difference, and all energies have been normalized to the value of $F(\pi)$ in the 0-junction configuration (the two leftmost plots). For all plots in this Figure: $\mu = 1$ eV, $\widetilde{\Delta} = 0.001$, $Z = 0$ and $x_1 k_F = 0$.

7. Results

In an effort to restrict our parameter space, we take our junction to have the parameter values $\mu = 1$ eV, $\widetilde{h} = 0.05$, $\widetilde{\Delta} = 0.001$, $x_1 k_F = 20$ and $x_2 k_F = 20$, corresponding to a short junction with exchange energy $h = 50$ meV and gap energy $\Delta = 1$ meV. Taking the exchange field felt by the conduction electrons to be about equal to the exchange field of the lattice electrons (up to $\approx 10^3$ T [27]) gives $h \approx 58$ meV, so our choice should not be unreasonable. BCS theory predicts an energy gap at zero temperature of about [14] $\Delta \approx 1.75 k_B T_c = 0.15 T_c$ meV K^{-1} where T_c is the critical temperature, which corresponds to our chosen gap energy for a T_c of about 7 Kelvin. We consider a low temperature for which $\Delta = 10 k_B T$, i.e. the gap energy is significantly larger than that of thermal fluctuations. Taking the effective quasiparticle mass to be equal to the electron mass ($m = m_e$) gives junction element lengths $x_1 = x_2 \approx 4$ nm, which roughly corresponds to the exchange lengths for transition metals we quoted in Chapter 3 and should thus be permissible within our single domain approximation for the ferromagnet.

We will primarily be interested in the variations with changing magnetization direction and superconducting phase. Secondly, we will be interested in the effect of different barrier transparencies and varying strength of the Rashba parameter. Again taking $m = m_e$, the Rashba parameter values we reported in Chapter 4 give our dimensionless parameter values approximately given by the range $0.001 \leq \widetilde{\alpha} \leq 0.1$. For our magnetic element, we take the saturation magnetization as $M_s = 1.3 \times 10^6$ A/m and the anisotropy constant as $K = 10^3$ J/m^3, as applicable to e.g. Fe-Ni alloys at about 40% Ni [49].

7.1 Free energy

For a an intermediate strength barrier $Z = 0.5$ and a Rashba coupling of strength $\widetilde{\alpha} = 0.1$ our numerical solutions for the free energy produce the plots in Figure 7.1, where we have chosen z as the polar axis and expressed the magnetization direction by the polar θ_m and azimuthal ϕ_m angles. The results for the four different phase values were all curve-fitted to an equation on the form $F = a - b\cos^2\theta_m + cf(\phi_m)$

yielding excellent correspondence, with root mean square errors on the order of 10^{-5}. Several functions were tried for the azimuthal dependence $f(\phi_m)$, ranging from a simple linear relation to trigonometric functions, all of which produced a negligible (by many orders of magnitude) value for c, suggesting a free energy that is azimuthally symmetric in the magnetization direction. This makes intuitive sense, as our model only has spin space isotropy broken only along the z-axis (i.e. the z-direction is the only privileged direction in spin space). These results indicate that the effect of the Andreev bound states is simply an easy z-axis: a free energy density proportional to the negative square of the z-component of the magnetization ($\cos^2\theta_m = m_z^2$) yields an effective field in the z-direction proportional to m_z. The values for the parameters $a < 0$ and $b > 0$ varied with phase in a way that is symmetric about $\Delta\phi = \pi$, as can be seen in the figure as the plots are pairwise identical.

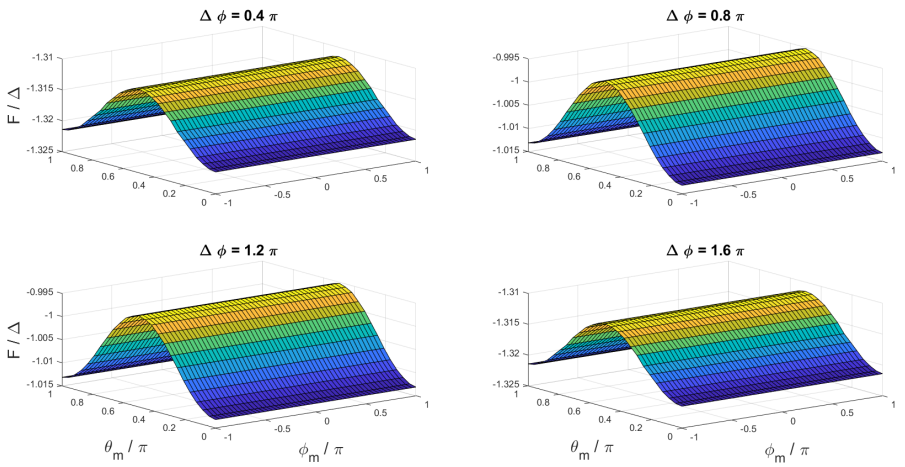

Figure 7.1: Free energy of Andreev bound state system plotted as a function of magnetization direction for different values of superconducting phase $\Delta\phi$. The z-axis is chosen to be the polar axis, and the magnetization direction is given by its polar (θ_m) and azimuthal (ϕ_m) angles. The free energy appears to be indifferent to the azimuthal angle, while under variation of the polar angle it attains minima along the z-axis and maxima in the xy-plane. The effect of changing the phase difference in the superconductors appears to be a shift of the total energy and a scaling of the θ_m dependence. For these plots $\mu = 1$ eV, $\widetilde{h} = 0.05$, $\widetilde{\Delta} = 0.001$, $\widetilde{\alpha} = 0.1$, $Z = 0.5$, $x_1 k_F = 20$ and $x_2 k_F = 20$.

Ideally, since it appears to be indifferent to ϕ_m, we would like to plot the free energy as a function of superconducting phase and polar magnetization angle. Unfortunately, as can be seen in Figure 7.2 the variation with changing phase is so large that it almost renders the smaller variation with polar angle indiscernible. However, the resulting plots contain interesting information on the phase dependence of our free energy, which for $Z = 0$ and $Z = 0.5$ clearly differs from that of the traditional

Josephson junction, as evidenced by the dip in free energy at $\Delta\phi = \pi$. Interestingly, the higher harmonic contributions responsible for the dip seem to be suppressed at $Z = 1$.

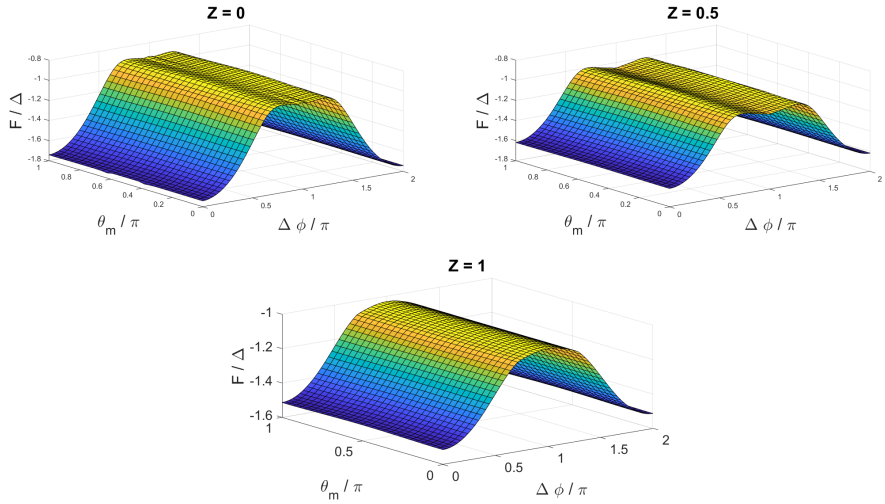

Figure 7.2: Free energy of Andreev bound state system plotted as a function of polar magnetization angle θ_m and phase difference $\Delta\phi$ between the superconductors for different values of the barrier strength Z. The variation with θ_m is so small compared to the effect of changing phase that it is difficult to see. For these plots $\mu = 1$ eV, $\widetilde{h} = 0.05$, $\widetilde{\Delta} = 0.001$, $\widetilde{\alpha} = 0.1$, $x_1 k_F = 20$ and $x_2 k_F = 20$.

To be able to visualize more clearly how the variation with θ_m depends on the phase, we want to repeat the calculations used in Figure 7.2, only for each phase value $\Delta\phi_n$ we subtract from the free energy the value $F(\Delta\phi_n, \theta_0)$ where θ_0 is the smallest polar angle used in our calculations. This effectively subtracts the variation in energy that is independent of magnetization direction. However, in doing this we have moved to an energy scale where the numerical errors due to energy levels becoming degenerate are significant. In addition to the degeneracies seen in Figure 6.2, we will for $Z = 0$ also have pairs of degeneracies around $\Delta\phi = \pi$ and at $\Delta\phi = 0$, as can be seen from the energy levels plotted in Figure 7.3.

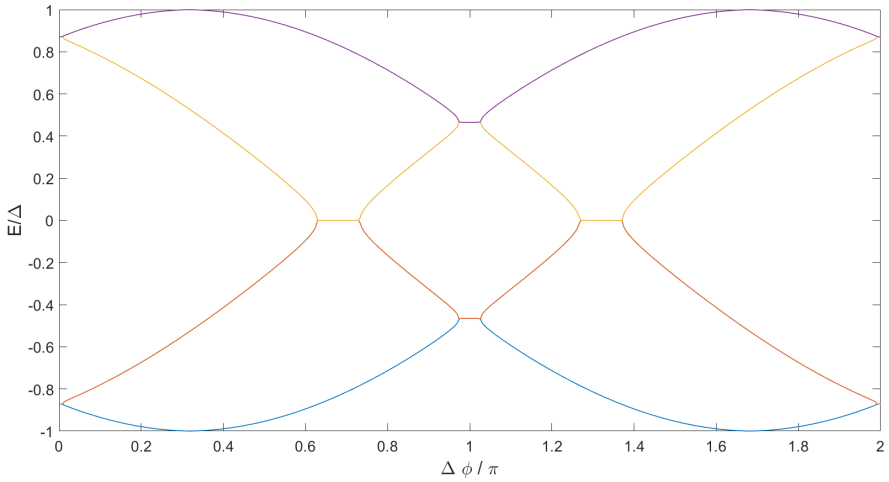

Figure 7.3: Plot of Andreev bound state energies as a function of superconducting phase $\Delta\phi$ for transparent barriers, i.e. $Z = 0$. In addition to the degeneracies seen in Figure 6.2, we also have pairs of degenerate energy levels at $\Delta\phi = \pi$ and $\Delta\phi = 0$. For this plot $\mu = 1$ eV, $\widetilde{h} = 0.05$, $\widetilde{\Delta} = 0.001$, $\widetilde{\alpha} = 0.1$, $x_1 k_F = 20$ and $x_2 k_F = 20$.

Using Figures 6.2 and 7.3 as guides, we simply exclude the phase intervals where degeneracies must be expected to introduce errors, with the hope that the remaining data will be sufficient to reveal how the θ_m dependence is affected by superconducting phase. Unfortunately, the energy levels for $Z = 1$ are degenerate over a significant phase interval and have therefore been excluded in the following. The resulting plot can be seen in Figure 7.4. Interestingly, we see that the free energy dependence on polar angle does not disappear for zero phase, leaving a minimum strength for the ABS easy axis that is about a fourth of the peak strength. The effect of increased barrier strength appears to be a flattening of the variation along $\Delta\phi$, somewhat decreasing the strength of the ABS easy axis around $\Delta\phi = \pi$ and slightly increasing it at zero phase. A repetition of these calculations with the Rashba parameter reduced by an order of magnitude ($\widetilde{\alpha} = 0.01$) produced results that were close to identical in form, but about two orders of magnitude smaller, suggesting that the strength of Rashba SOC influences only the magnitude of the effects we have found.

Both sets of results displayed in Figure 7.4 were curve fitted to an equation on the form

$$F = \sin^2\theta_m \Big[c_0 + \sum_{n=1}^{N} c_n \cos n\Delta\phi \Big] \tag{7.1}$$

and both achieved a tolerable fit (root mean square errors of about 10^{-4}) at the

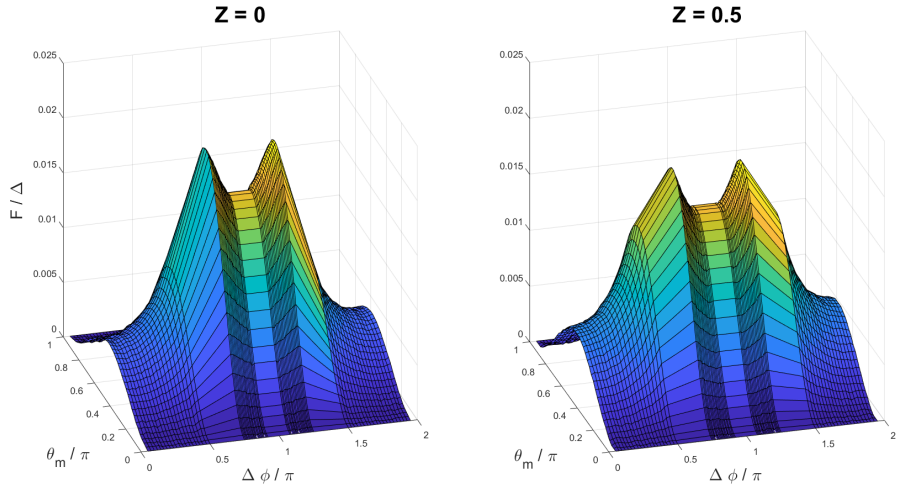

Figure 7.4: Free energy of Andreev bound state system with the part dependent only on phase subtracted, plotted as a function of polar magnetization angle θ_m and phase difference between the superconductors $\Delta\phi$. The intervals with no data points correspond to parameter values for which we know that the numerical scheme introduces significant errors. For this plot $\mu = 1$ eV, $\widetilde{h} = 0.05$, $\widetilde{\Delta} = 0.001$, $\widetilde{\alpha} = 0.1$, $x_1 k_F = 20$ and $x_2 k_F = 20$.

inclusion of four cosine terms. Including higher order terms further improved the fit, reinforcing the earlier indication that the ABS effective field takes the form of an easy z-axis (since $\sin^2\theta_m = 1 - m_z^2$). If we can find a function $f(\Delta\phi)$ that approximates the phase dependent factor (i.e. the bracketed part of (7.1)), our effective field will take the form

$$\boldsymbol{h}_{\text{ABS}} = -C\frac{\partial F}{\partial \boldsymbol{m}} = 2m_z C f(\Delta\phi) \tag{7.2}$$

where C is the constant denoting the proportionality of our calculated free energy to the relevant free energy density in the ferromagnet, yet to be discussed. We note that $f(\Delta\phi)$ has unit energy, making the expression dimensionless as it should be. To find suggestions for $f(\Delta\phi)$, we perform a curve fitting for numerical results with $\theta_m = \pi/2$ varying the number of cosine terms used. The results for attempts with four and six cosine terms are plotted in Figure 7.5, and from these we expect the curve fit with six cosine terms to be a good approximation and will use it for our $f(\Delta\phi)$.

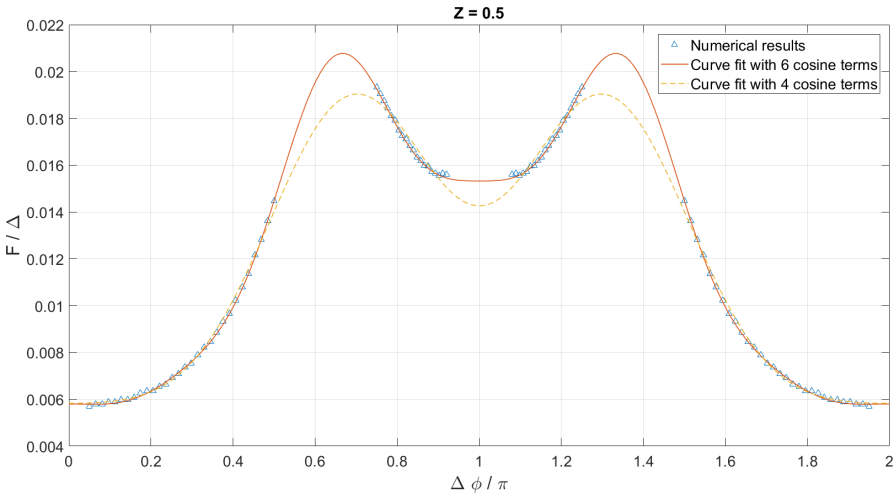

Figure 7.5: Strength of easy axis ABS effective field as a function of phase (calculated as $F(\Delta\phi) = F(\Delta\phi, \pi/2) - F(\Delta\phi, 0)$ where the second variable is polar magnetization angle) together with analytical functions found by curve fitting a series with four and six cosine terms, respectively. The three intervals with no numerical results correspond to parameter values for which we know that the numerical scheme introduces significant errors. For this plot $\mu = 1$ eV, $\widetilde{h} = 0.05$, $\widetilde{\Delta} = 0.001$, $\widetilde{\alpha} = 0.1$, $x_1 k_F = 20$ and $x_2 k_F = 20$.

As another data point to assess the effect of increased barrier strength, we perform the procedure used in Figure 7.4 for $Z = 0.8$, for which we do not have the same numerical difficulties as with $Z = 1$. The result can be seen in Figure 7.6. Also here the dependence on θ_m fits perfectly with the form of an easy axis, but now there is almost no variation with superconducting phase. We are left with an easy axis of approximately constant strength, a bit higher than the $\Delta\phi = 0$ strength observed for weaker barriers. This could suggest that the phase dependent part of the easy axis strength is due to a process requiring Andreev reflections (which are suppressed in favor of normal reflections by stronger barriers), while the phase independent part is largely unaffected by barrier strength. This would be the case if, for instance, the phase dependent part is due to the supercurrent through the junction, while the phase independent part is the result of a population of quasiparticles reflected back and forth at equal rates so as to create zero net current. Such a population of quasiparticle could be the result of equal numbers of Andreev reflections in each direction (as would have to be the case for $Z = 0$ where normal reflection vanishes) and it could be due to quasiparticles trapped in the junction by normal reflection at the interfaces (as would have to be the case with barriers strong enough to prohibit Andreev reflection). In the general case we would assume that both these processes contribute to this equilibrium population of quasiparticles.

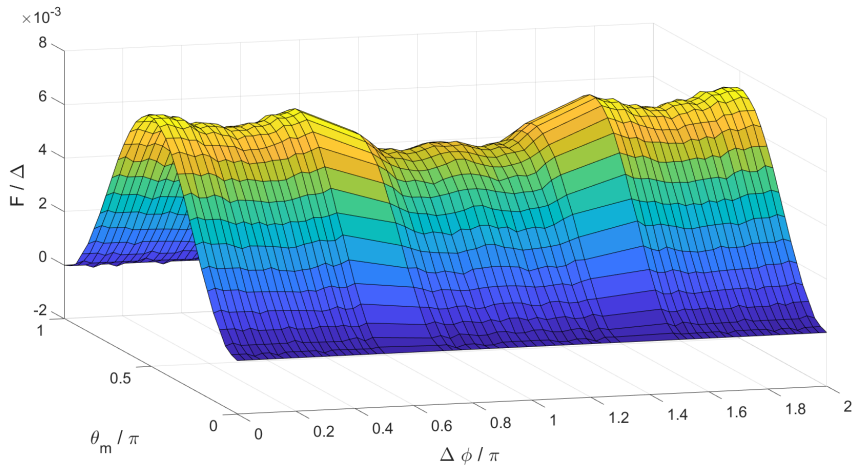

Figure 7.6: Free energy of Andreev bound state system with the part dependent only on phase subtracted, plotted as a function of polar magnetization angle θ_m and phase difference between the superconductors $\Delta\phi$. The intervals with no data points correspond to parameter values for which we know that the numerical scheme introduces significant errors. For this plot $Z = 0.8$, $\mu = 1$ eV, $\widetilde{h} = 0.05$, $\widetilde{\Delta} = 0.001$, $\widetilde{\alpha} = 0.1$, $x_1 k_F = 20$ and $x_2 k_F = 20$.

7.2 Magnetization dynamics

If we would like to apply our results for the free energy and corresponding effective field to a dynamically evolving system, we must consider the applicability of our quasi-static approach: for how rapid change in the system will our static solutions for the BTK wave functions be valid? The smallest energy scale in our system is the gap energy $\Delta = 1$ meV, so the time evolution of a dynamic system can be seen as an adiabatic perturbation as long as it evolves on a time scale τ fulfilling $\hbar/\tau \ll \Delta$. If, for instance, our magnet has an easy axis anisotropy with anisotropy constant K and is disturbed from equilibrium, the magnetization will spiral towards the easy axis with a precession frequency (see Chapter 3):

$$\omega_P = \gamma |\boldsymbol{H}_\mathrm{a}| = \gamma \frac{2K}{M_s} \frac{M_\parallel}{M_s} \leq \gamma \frac{2K}{M_s} \tag{7.3}$$

where $M_\parallel$ is the magnetization component along the easy axis. The magnetic properties chosen for our ferromagnet give $\omega_P \approx 1/(3.5\text{ns})$, or equivalently $\hbar\omega_P \approx 0.001$ meV, safely within the bounds of our adiabatic approximation. A system with such an anisotropy (let's say along the y-axis) would be bistable and as such could be used as a magnetic bit, encoding information in the two stable magnetization directions (e.g. 1 for magnetization in the $\hat{y}$ direction and 0 for magnetization in the $-\hat{y}$ direction). We will be interested in whether an effective field on the form that we

have found for the Andreev bound states could be used to drive magnetic switching in such a system. Obviously, if the magnetization is strictly along the y-axis, our ABS easy axis would have no effect, regardless of its relative strength, since there is no magnetization component along the z-axis. However, we will assume that thermal excitations create small deviations from the equilibrium magnetization, and in absence of any other torques than that of the magnetic bit easy axis we take the magnetization to be in a tight precession (or a tight inward spiral if there is damping in the system) about one of the equilibria.

If we were to bias the junction with a voltage V_a, we would introduce a time evolution to the superconducting phase as we saw in Chapter 2: $\Delta\phi \to \Delta\phi_0 + \omega_J t$, where $\omega_J = \frac{2eV_a}{\hbar}$ is as before the Josephson frequency. In this way we could drive the phase dependent strength of our easy axis ABS effective field at a frequency of our choosing. However, the driving frequencies that will be of interest to us in provoking magnetic switching in the system are no larger than twice the maximum precession frequency of the magnetic bit easy axis, $\omega_J \leq 2\omega_P$, and are thus permissible within our adiabatic approximation. Frequencies in this range correspond to bias voltages on the order of 10^{-6} volt. Taking our junction to originally have zero phase difference between the superconductors, and applying a bias voltage at $t = 0$, we will have a total effective field

$$h_{\text{eff}} = h_a + h_{\text{ABS}}(t) = \frac{2K}{\mu_0 M_s^2} m_y + 2C m_z f\big(\Theta(t)\omega_J t\big) \tag{7.4}$$

where $\Theta(t)$ is the Heaviside step function and $f(\Delta\phi)$ is the six cosine term approximation to the phase dependence plotted in Figure 7.5. The dimensionless LLG-equation we derived in Chapter 3 is easily implemented and solved in MATLAB using the inbuilt ordinary differential equation solver ODE45. Choosing a Gilbert damping parameter of $\alpha = 0.01$ and an initial condition where the magnetization is close to $-\hat{y}$, for $C = 0.025/\Delta$ we are able to produce switching by choosing a driving frequency close to ω_P. The trajectory of the magnetization is plotted in Figure 7.7

Some trial and error was necessary to find a driving frequency that would produce switching given a certain value for C, as the dynamics are very sensitive to the exact position at the time we start driving the superconducting phase. For a slightly weaker ABS effective field, the magnetization had to be driven much more gradually away from the easy axis, an example of which can be seen in Figure 7.8 for $C = 0.02/\Delta$. While it might initially seem that even lower values for C should only require us to drive the system at resonance frequency for a little longer to achieve switching, this is unfortunately not the case: since the precession frequency of the magnetic bit easy axis is proportional to the x-component of magnetization, there is not one single frequency for us to target. Thus, if we choose a frequency that achieves resonance with the initial precession, we will increase the radius of

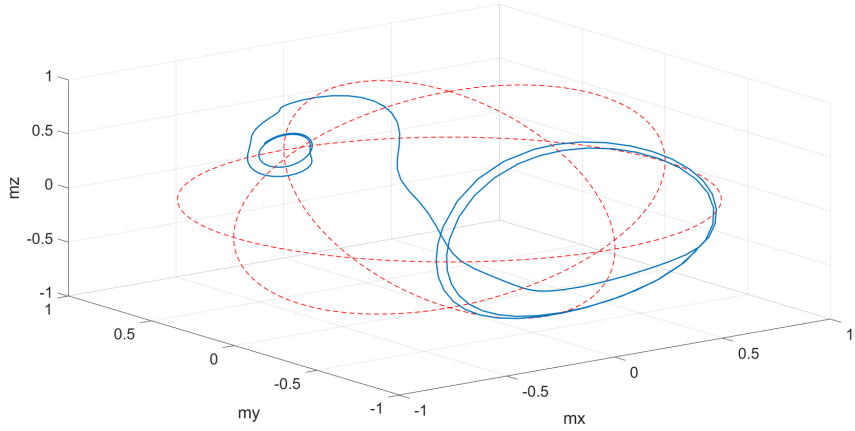

Figure 7.7: Magnetization trajectory for switching by ABS effective field. After a short time of precession about $\hat{y}$, we start to drive the superconducting phase at a frequency close to the frequency of precession, which drives the magnetization to the vicinity of the other stable direction. The phase is again set to zero, and the magnetization is left precessing around $-\hat{y}$. For this plot $\alpha = 0.01$, $C = 0.025/\Delta$ and the time taken is about 180 ns.

precession until our frequency is no longer close enough to the new precession frequency to have the desired effect. For $C = 0.01/\Delta$ we were unable to produce switching, even if we made the system dissipationless by removing Gilbert damping. For higher values of C, we are able to produce faster switching, but only up to a point: while $C = 0.05/\Delta$ allows slightly more expedient switching than does $C = 0.02/\Delta$, for $C = 0.1/\Delta$ the minimum ABS easy axis strength (i.e. the strength at $\Delta\phi = 0$) is enough to break the bistability of the easy y-axis (even for miniscule deviations from the stable direction) and we effectively no longer have a magnetic bit.

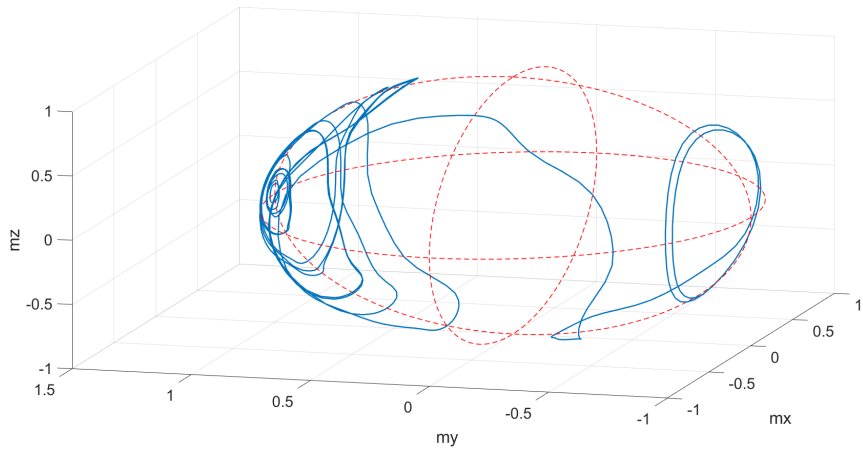

Figure 7.8: Magnetization trajectory for switching by ABS effective field. After a short time of precession about $\hat{y}$, we start to drive the superconducting phase at a frequency close to the frequency of precession, which drives the magnetization to the vicinity of the other stable direction. The phase is again set to zero, and the magnetization is left precessing around $-\hat{y}$. For this plot $\alpha = 0.01$, $C = 0.02/\Delta$ and the time taken is about 620 ns.

8. Discussion

In calculating our Andreev bound state free energy, we have considered only one-dimensional transport, and thus only a single propagation mode through the junction. However, as our system has some cross-sectional area, there will be a possibility of modes with $k_y, k_z \neq 0$. We will approximate the energy of these modes to be the same as for the one-dimensional transport mode (i.e. the F we have calculated). This is expected to be an overestimation, as the oblique angles of incidence produced by the transverse momenta will increase the rate of regular reflection at the interfaces and thus have an effect similar to that of increasing the barrier strength (i.e. suppressing Andreev reflection). Additionally, our energy splitting in the SOC element is proportional to the x-component of momentum, any momentum along the y-axis would have no effect on the energy splitting, while the z-component of momentum would change the axis along which spin is resolved in the SOC-element. We will neglect this effect, as we assume that our system is dominated by states with momentum predominantly along the x-axis.

To get some sense of the angle dependence of increased normal reflection at oblique incidence, we consider a toy model for an electron incident on an interface in the yz-plane with barrier strength Z (defined as before) between two normal metals. As we have momentum conservation parallel to the interface, we need only consider the dependence on $k_x = k_F \cos\theta$ where θ is the angle of incidence. Imposing the same constraints at the interface as in Chapter 5 and solving for the transmission probability gives:

$$T = \frac{1}{1 + \frac{Z^2}{4\cos\theta^2}} \tag{8.1}$$

For $Z = 1$ we reduce transmission by half for $\cos\theta = k_x/k_F = 1/2$, meaning we need k_x to be significantly smaller than k_F to effectively suppress transmission. However, as each Andreev reflection requires two regular transmissions (and Andreev bound states processes might in turn demand multiple Andreev reflections) is seems reasonable that the effects we are interested in (i.e. the phase dependent part of the easy axis strength) would scale with some higher power of T. Regard-

less, we can see from (8.1) that (for finite Z) any modes with transverse momenta approaching the Fermi momentum (so that k_x/k_F becomes small) can be safely neglected on the grounds that they are unlikely to allow Andreev reflection.

Taking a simple particle-in-a-box approach to the transverse modes, we can only have the discrete set of transverse momenta

$$k_y = \frac{n_y \pi}{L_y} \qquad k_z = \frac{n_z \pi}{L_z} \tag{8.2}$$

where L_y and L_z are the ferromagnet thickness and width, respectively. The momenta are of course subject to the constraint

$$k_y^2 + k_z^2 < k_F^2 \qquad \text{so that} \qquad n_{y(z)} < \frac{k_F L_{y(z)}}{\pi} \tag{8.3}$$

i.e. there must be some momentum in the x-direction for the modes to propagate at all. We see that for an L_y on the order of $k_F L_y \approx \pi$, there will be only one non-zero y-mode, which we can safely ignore since $k_y \approx k_F$. Thus transport in the junction is essentially two dimensional in this case. The number of transverse modes will be almost $n_z = k_F L_z/\pi$, and our proportionality constant for the effective field becomes:

$$C = \frac{1}{V}\frac{F_{\text{ABS}}}{F}\frac{1}{\mu_0 M_s^2} = \frac{1}{x_2 L_y L_z}\frac{k_F L_z}{\pi}\frac{1}{\mu_0 M_s^2} = \frac{k_F^3}{\pi^2}\frac{1}{x_2 k_F}\frac{1}{\mu_0 M_s^2} \tag{8.4}$$

where we have used $L_y \approx \pi/k_F$. For the parameter values used in Chapter 7 ($\mu = 1$eV, $x_2 k_F = 20$, and taking the effective mass to be simply the electron mass) gives us a value

$$C \approx 3.2 \times 10^{20}\ \text{J}^{-1} \approx \frac{0.05}{\Delta} \tag{8.5}$$

However, the thickness we have used is comparable to the lattice parameter of transition metals (typically a few Ångström [27]) at $L_y \approx 6$ Å, so we cannot readily expect all our results for bulk ferromagnets to apply. Going to the 2D-case requires us to substitute areas for volumes, both in the energy density and the saturation magnetization (magnetic moment per volume). However, only one of the two factors of M_s got into our expression for C as a normalization of magnetization, the other one originated as a normalization of the effective field. The effective field retains the unit energy per magnetic moment, and thus must still be normalized by (the 3D) M_s. It might seem the 3D saturation magnetization should not affect the 2D problem, and indeed it does not: it serves only as a convenient normalization of the effective field that also sets the time scale of the problem, leaving the dynamics unchanged. We are thus left with

$$C = \frac{1}{A}\frac{F_{\text{ABS}}}{F}\frac{1}{\mu_0 M_s M_{2D}} = \frac{1}{x_2 L_z}\frac{k_F L_z}{\pi}\frac{1}{\mu_0 M_s M_{2D}} = \frac{k_F^2}{\pi}\frac{1}{x_2 k_F}\frac{1}{\mu_0 M_s M_{2D}} \tag{8.6}$$

where M_{2D} is the saturation magnetization of our 2D magnet. As a first approximation, we can take M_{2D} to be equal to the bulk saturation magnetization multiplied by the thickness of a single atomic layer: $M_{2D} \approx M_s L_{\text{layer}}$. While we should expect this to be an overestimation of the saturation magnetization for an actual monolayer (since there are fewer nearest neighbors to exert an exchange field on each spin), we can expect it to be an adequate model for e.g. a stack of weakly coupled magnetic monolayers. Such a stack would retain many of the properties of the bulk ferromagnet but would essentially allow only 2D electron transport and as such fits well with our model. This approximation for M_{2D} simply gives us back the 3D expression for C, only with L_{layer} in place of L_y. As we saw that L_y should be of the same order of magnitude as the lattice parameter (and thus L_{layer}), so as a first approximation we simply use the expression (8.4) for the proportionality constant.

8.1 Potential for technological application

In the introduction, we touted the advantages of manipulating magnetic memory without the use of a conventional current. We have shown that for an example system, it should be possible to achieve switching of a magnetic bit through application of a voltage bias to the junction, which can be assumed to produce only negligible conventional currents at low temperature. Although the ability to perform switching was limited to a somewhat restricted interval of values for the proportionality constant C (which we were only able to calculate a first approximation for), it seems plausible that combinations of materials and junction parameters exist for which switching is indeed possible.

Assuming that magnetic switching by ABS effective field is achievable, we could imagine that the ferromagnetic element in our junction is incorporated in a magnetic tunnel junction (i.e. an F-I-F junction in which large differences in tunneling resistance occur for parallel and antiparallel magnetizations in the two magnetic elements [50, 51]) to facilitate reading the state of our magnetic bit. Compared to writing methods using applied magnetic fields or spin polarized currents, such a magnetic memory unit would have the (significant) advantage of writing without the use of a conventional current. However, it would present other difficulties, the least of which might be the cryogenic cooling required for the superconductive elements. Since the resulting effective field is an easy axis, the exact timing of our bias voltage would decide whether switching occurs as the ABS effective field could eas-

ily drive the magnetization back and forth between the two states of the magnetic bit. Contrast this with the application of an external field: for a strong enough applied field, we simply have to wait long enough for switching to occur and we will be guaranteed that the magnetization is in the direction of the external field. Another weakness in the proposed system stems from the fact that the ABS effective field we have found cannot be set to zero strength by manipulation of superconducting phase. Thus, any such field of a comparable strength with the magnetic bit easy axis would introduce a constant easy axis in competition to that of the magnetic bit which would effectively reduce the regions of stability from essentially the two halves of the magnetization sphere ($m_x > 0$ and $m_x < 0$) to two cones centered on the two stable directions ($m_x > c$ and $m_x < -c$ for some $0 < c < 1$). This effect can be seen in the magnetization trajectory plotted in Figure 8.1. Also taking into account that we must have some deviation from the stable magnetization directions of the magnetic bit for the ABS effective field to have any effect, we could imagine that the proposed system could encounter problems with poor bit stability.

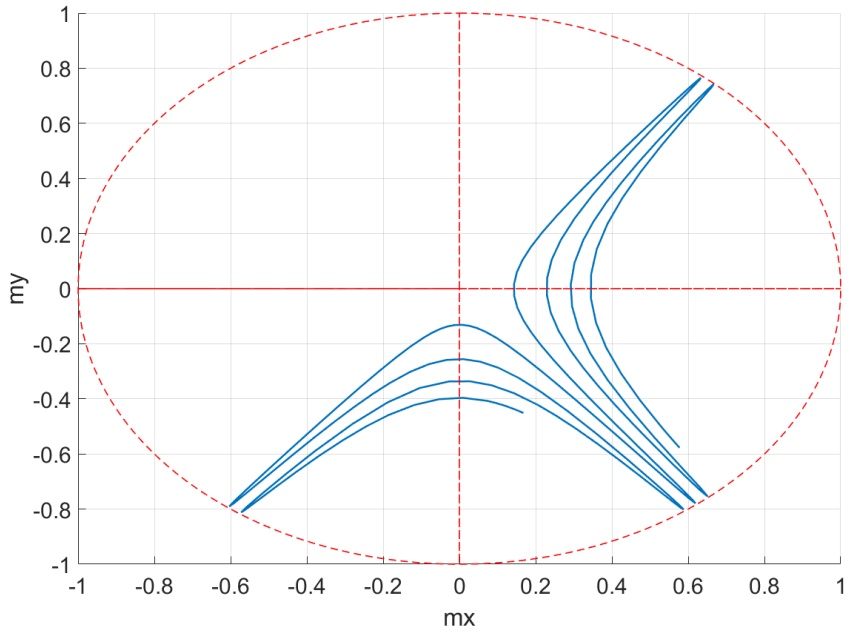

Figure 8.1: Magnetization trajectory with no driving of the ABS effective field. The magnetization is initiated in the lower right quadrant ($m_x = -m_y = m_z$) from where it would, in absence of the ABS effective field, spiral towards $m_y = -1$. However, the minimum ($\Delta\phi = 0$) strength of the ABS easy axis is sufficient that the magnetization instead goes into a skewed outward spiral from $m_x = 1$ until it reaches the attractive cone around one of the stable positions of the magnetic bit easy axis. For this plot $\alpha = 0.01$, $C = 0.05/\Delta$ and the time taken is about 260 ns.

9. Concluding remarks

We have demonstrated that an extended BTK formalism can be used to find the magnetization dependent energy levels of Andreev bound states in a version of the Josephson junction incorporating a ferromagnet and an element displaying Rashba spin-orbit coupling. We have shown that the resulting free energy for a range of example systems takes the form of an easy axis effective field perpendicular to both the direction of propagation in the junction and the direction of broken inversion symmetry responsible for Rashba SOC. In one example system it was demonstrated that manipulation of the easy axis strength could be achieved by oscillation of the superconducting phase induced by a bias voltage imposed on the junction, and that this effect could be used to perform the switching of a magnetic bit.

Although such switching without the use of a conventional current could be construed as a step toward dissipationless magnetic memory technology, we have argued that such a method for switching is fundamentally flawed for applications in magnetic memory. Chief among our concerns was the fact that application of an easy axis (e.g. perpendicular to the stable magnetization directions of the magnetic bit) cannot be guaranteed to achieve switching (or rather an odd number of switches) of the bit except by exact timing of the application. Such timing would have to account for the initial deviation of the magnetization from a stable direction assumed to be the result of thermal fluctuations, which does not seem plausibly achievable for technological application.

However, the base mechanism we have demonstrated, namely the lifting of spin degeneracy in an S-F-S junction by introduction of a spin-orbit coupled element, can still be of interest to future applications in spintronics, and systems similar to ours warrant further investigation. One such example could be an S-F-S junction where one or both interfaces consist of a layer of heavy metal displaying Rashba SOC. Such a junction could be investigated by the very methods we have employed, with the exception that one would have to consider three-dimensional transport explicitly, incurring an integration over angles of incidence at the barriers.

Bibliography

[1] E. K. W. Wold. *Toward superconductive magnetization dynamics*. Unpublished project thesis, NTNU, 2017.

[2] M. Eschrig. Spin-polarized supercurrents for spintronics. *Phys. Today*, 64(1):43, 2011.

[3] I. Žutić, J. Fabian, and S. Das Sarma. Spintronics: Fundamentals and applications. *Rev. Mod. Phys.*, 76:323, Apr 2004.

[4] S. A. Wolf, D. D Awschalom, R. A. Buhrman, J. M. Daughton, S. Von Molnar, M. L. Roukes, A. Yu. Chtchelkanova, and D. M. Treger. Spintronics: a spin-based electronics vision for the future. *Science*, 294(5546):1488, 2001.

[5] T. Yamashita, K. Tanikawa, S. Takahashi, and S. Maekawa. Superconducting π qubit with a ferromagnetic josephson junction. *Phys. Rev. Lett.*, 95:097001, 2005.

[6] A. Brataas, A. D. Kent, and H. Ohno. Current-induced torques in magnetic materials. *Nature materials*, 11(5):372, 2012.

[7] L. Berger. Emission of spin waves by a magnetic multilayer traversed by a current. *Physical Review B*, 54(13):9353, 1996.

[8] J. C. Slonczewski. Current-driven excitation of magnetic multilayers. *Journal of Magnetism and Magnetic Materials*, 159(1):L1, 1996.

[9] K. J. O'Dwyer and D. Malone. Bitcoin mining and its energy footprint. 2014.

[10] H. K. Onnes. The resistance of pure mercury at helium temperatures. *Commun. Phys. Lab. Univ. Leiden*, 12(120):1, 1911.

[11] W. Meissner and R. Ochsenfeld. Ein neuer effekt bei eintritt der supraleitfähigkeit. *Naturwissenschaften*, 21(44):787, 1933.

[12] L. N. Cooper. Bound electron pairs in a degenerate fermi gas. *Physical Review*, 104(4):1189, 1956.

[13] J. Bardeen, L. N. Cooper, and J. R. Schrieffer. Microscopic theory of superconductivity. *Physical Review*, 106(1):162, 1957.

[14] J. Bardeen, L. N. Cooper, and J. R. Schrieffer. Theory of superconductivity. *Physical Review*, 108(5):1175, 1957.

[15] K. Fossheim and A. Sudbø. *Superconductivity: Physics and Applications*. John Wiley & Sons, 2004.

[16] A. L. Fetter and J. D. Walecka. *Quantum theory of many-particle systems*. Courier Corporation, dover edition, 2014.

[17] N.N. Bogoliubov. A new method in the theory of superconductivity. iii. *Sov. Phys. JETP*, 7(1):51, 1958.

[18] G. E. Blonder, M. Tinkham, and T. M. Klapwijk. Transition from metallic to tunneling regimes in superconducting microconstrictions: Excess current, charge imbalance, and supercurrent conversion. *Physical Review B*, 25(7):4515, 1982.

[19] I. Giaever. Energy gap in superconductors measured by electron tunneling. *Physical Review Letters*, 5(4):147, 1960.

[20] I. Giaever. Electron tunneling between two superconductors. *Physical Review Letters*, 5(10):464, 1960.

[21] B. D. Josephson. Possible new effects in superconductive tunnelling. *Physics letters*, 1(7):251, 1962.

[22] R. P. Feynman, R. B. Leighton, and M. Sands. *The Feynman lectures on physics, vol. III*. Addison-Wesley, 1965.

[23] D. B. Szombati, S. Nadj-Perge, D. Car, S. R. Plissard, E. P. A. M. Bakkers, and L. P. Kouwenhoven. Josephson ϕ_0-junction in nanowire quantum dots. *Nature Physics*, 12(6):568, 2016.

[24] A. F. Andreev. The thermal conductivity of the intermediate state in superconductors. *Sov. Phys. JETP*, 19(5):1828, 1964.

[25] C. Zener. Interaction between the d shells in the transition metals. *Physical Review*, 81(3):440, 1951.

[26] P. Curie. *Propriétés magnétiques des corps a diverses températures*. Gauthier-Villars et fils, 1895.

[27] C. Kittel. *Introduction to solid state physics*. Wiley, eighth edition, 2005.

[28] D. J. Griffiths. *Introduction to quantum mechanics*. Cambridge University Press, 2016.

[29] L. Landau and E. Lifshitz. On the theory of the dispersion of magnetic permeability in ferromagnetic bodies. *Phys. Z. Sowjetunion*, 8(153):101, 1935.

[30] T. L. Gilbert. A phenomenological theory of damping in ferromagnetic materials. *IEEE Transactions on Magnetics*, 40(6):3443, 2004.

[31] P. A. M. Dirac. On the theory of quantum mechanics. *Proceedings of the Royal Society of London A: Mathematical, Physical and Engineering Sciences*, 112(762):661, 1926.

[32] G. S. Abo, Y. Hong, J. Park, J. Lee, W. Lee, and B. Choi. Definition of magnetic exchange length. *IEEE Transactions on Magnetics*, 49(8):4937, 2013.

[33] E. C. Stoner and E. P. Wohlfarth. A mechanism of magnetic hysteresis in heterogeneous alloys. *Philosophical Transactions of the Royal Society of London A: Mathematical, Physical and Engineering Sciences*, 240(826):599, 1948.

[34] C. Kittel. Physical theory of ferromagnetic domains. *Reviews of modern Physics*, 21(4):541, 1949.

[35] D. J. Griffiths. *Introduction to electrodynamics*. Pearson Education, third, international edition, 2008.

[36] Y. A. Bychkov and E. I. Rashba. Oscillatory effects and the magnetic susceptibility of carriers in inversion layers. *Journal of physics C: Solid state physics*, 17(33):6039, 1984.

[37] A. D. Caviglia, M. Gabay, S. Gariglio, N. Reyren, C. Cancellieri, and J.-M. Triscone. Tunable rashba spin-orbit interaction at oxide interfaces. *Physical review letters*, 104(12):126803, 2010.

[38] S. LaShell, B. A. McDougall, and E. Jensen. Spin splitting of an au (111) surface state band observed with angle resolved photoelectron spectroscopy. *Physical review letters*, 77(16):3419, 1996.

[39] Yu. M. Koroteev, G. Bihlmayer, J. E. Gayone, E. V. Chulkov, S. Blügel, P. M. Echenique, and Ph. Hofmann. Strong spin-orbit splitting on bi surfaces. *Phys. Rev. Lett.*, 93:046403, 2004.

[40] C. R. Ast, J. Henk, A. Ernst, L. Moreschini, M. C. Falub, D. Pacilé, P. Bruno, K. Kern, and M. Grioni. Giant spin splitting through surface alloying. *Physical review letters*, 98(18):186807, 2007.

[41] J. O. Andersen. *Introduction to statistical mechanics*. Akademika forlag, 2012.

[42] A. A. Golubov, M. Yu. Kupriyanov, and E. Il'Ichev. The current-phase relation in josephson junctions. *Reviews of modern physics*, 76(2):411, 2004.

[43] A. Buzdin. Direct coupling between magnetism and superconducting current in the josephson φ_0 junction. *Phys. Rev. Lett.*, 101:107005, Sep 2008.

[44] W. Haberkorn, H. Knauer, and J. Richter. A theoretical study of the current-phase relation in josephson contacts. *physica status solidi (a)*, 47(2), 1978.

[45] G. Annunziata, H. Enoksen, J. Linder, M. Cuoco, C. Noce, and A. Sudbø. Josephson effect in s/f/s junctions: Spin bandwidth asymmetry versus stoner exchange. *Physical Review B*, 83(14):144520, 2011.

[46] A. I. Buzdin, L. N. Bulaevskii, and S. V. Panyukov. Critical-current oscillations as a function of the exchange field and thickness of the ferromagnetic metal (f) in an sfs josephson junction. *JETP Lett*, 35(4):147, 1982.

[47] V. V. Ryazanov, V. A. Oboznov, A. Yu. Rusanov, A. V. Veretennikov, A. A. Golubov, and J. Aarts. Coupling of two superconductors through a ferromagnet: Evidence for a π junction. *Physical review letters*, 86(11):2427, 2001.

[48] A. I. Buzdin and M. Yu. Kupriyanov. Josephson junction with a ferromagnetic layer. *JETP Lett*, 53(6):321, 1991.

[49] Werner Martienssen and Hans Warlimont. *Springer handbook of condensed matter and materials data*. Springer Science & Business Media, 2005.

[50] T. Miyazaki and N. Tezuka. Giant magnetic tunneling effect in fe/al2o3/fe junction. *Journal of Magnetism and Magnetic Materials*, 139(3):L231, 1995.

[51] J. S. Moodera, L. R. Kinder, T. M. Wong, and R. Meservey. Large magnetoresistance at room temperature in ferromagnetic thin film tunnel junctions. *Phys. Rev. Lett.*, 74:3273, Apr 1995.